

## Reply to the Comments to the Author

by Johannes Hepp & co-authors

Dear Marcel van der Meer,

first of all, I want to express my gratefulness about your constructive handling of our manuscript and that we had the possibility to revise also our replies the referees. Second, I want to thank you for raising the constructive suggestions in the comments to the authors. Please find our replies to your issues below.

*First of all I would like to thank you for this reply to the reviewers comments, much better than the original reply. I also want to thank the reviewers again for their reviews. I totally agree with you that the limited amount people doing this combined approach should not affect your development and application of the proxy in anyway. That being said, I do see the point of the reviewers as well. I guess the measurements are quite tricky and you have to make quite a few assumptions, like a fixed  $\delta_{bio}$ , to make this work. All and all maybe not so convincing yet for other users to get involved in, with the emphasis on yet. I do see the advantage of this combined approach. Of course hydrogen and oxygen behave very similarly with respect to humidity, temperature, evaporation etc. and I can't really judge if that is good or bad. There are benefits to independent proxies, say hydrogen isotopes from organic molecules and oxygen isotopes from inorganic carbonates for instance.*

*Of course you did measure completely independent proxies for temperature and pH, but these are not linked to the isotope results in anyway? Is there anything you say based on the isotope data that can be back-up by the GDGT data? Something about the local (micro) climate being different from that of the weather stations, for instance? The GDGTs were measured on the same samples as the isotopes, they should reflect the same "micro" climate. Or the underestimation of the RH, can that be linked/supported by some of the other results? Just to link the two independent methods a bit more together?*

- ➔ Thank you for raising that important issue and for you suggestions how to link the both proxy types presented in the study closer together. Since the GDGTs are produced (or originate) mainly from microorganisms in the soil and the (long-chain) *n*-alkanes and the (hemicellulose) sugars are known to be produced by plants (mainly higher terrestrial plants when considering the homologues/compounds which we focus on), it is not that simple to find connections between those datasets, besides they are synthesized in the same environment. That's the reason why we decide to interpret the proxy results separately in the current manuscript. However, when looking on the correlation between reconstructed and "measured"  $T_{MA}$ , the relationship based on the data achieved from our study would be rather weak. But when the our data is plotted together with the large (world wide) dataset from Peterse et al. (2012), our data fits well to the overall correlation (Fig. 6A). The reconstructions based on the isotope data have therefore to tackle the same issue regarding a rather small data set and rather medium changes along our transect with regard to the climate conditions. That's probably a link

between the GDGT-based reconstructions and the isotope-based one. We will add a respective sentence to the conclusion to have a connection between the GDGT part and the isotope part. However, besides the correlation between reconstructed source water isotope composition and RH to measured values is rather weak due to the rather small range which covers the transect data, the main issue here is that the data plot partly not well on the 1:1 line, which should be the case if the idea behind the proxy calculations are right. That's why we intensively discuss the influence of different vegetation types on our isotope proxy results. That's still something what does obviously not affect the GDGTs, which is also interesting. We will add therefore a respective sentence to highlight this finding in the conclusion as well as in the abstract.

*The other thing I was thinking about is that, since the water isotopes behave so similarly you could use the combined measurements to examine, for instance,  $\delta$ bio. Flip your proxy around so to say. Plenty of options for future work, I think.*

- ➔ Thank you for raising that inspiring issue. We think that would be a good project for a further study because it would be nice to combine here all available compound-specific isotope (terrestrial *n*-alkanes as well as sugars) and try to parameterize the model based on measured data. One could for example use a kind of model presented by Konecky et al. (2019) and expand it to (hemicellulose) sugars and cellulose.

*I have a few minor comments; You mention in your response and in the discussion that you cannot see the difference between damping or differences in  $\delta$ bio, this has been left out of the abstract?*

- ➔ Thank you for that constructive comment. That was just a mistake. We will add this as it is mentioned in the conclusions.

*In the introduction you mention quite a few variables on which the hydrogen isotopic composition of *n*-alkanes depend, some of these are what you would like to reconstruct, so that is not a bad thing right?*

- ➔ Yes, you are right. All those factors are included in the isotope equations and thus in the isotope proxy calculations/reconstructions.

*In the figure 1 legend you mention that the map is sourced by the US National Park Service (just checking)?*

- ➔ Yes, that's correct.

In line 351 after the, it says "precipitation drops .... " I don't see how this is linked to the rest of this sentence?

→ You are right, this is now corrected to “when precipitation amount drops below 700-800 mm.””.

## Literature

Konecky, B., Dee, S. G. and Noone, D. C.: WaxPSM: A Forward Model of Leaf Wax Hydrogen Isotope Ratios to Bridge Proxy and Model Estimates of Past Climate, *Journal of Geophysical Research: Biogeosciences*, 124, 2107–2125, doi:10.1029/2018JG004708, 2019.

Peterse, F., van der Meer, J., Schouten, S., Weijers, J. W. H., Fierer, N., Jackson, R. B., Kim, J. H. and Sinninghe Damsté, J. S.: Revised calibration of the MBT-CBT paleotemperature proxy based on branched tetraether membrane lipids in surface soils, *Geochimica et Cosmochimica Acta*, 96, 215–229, doi:10.1016/j.gca.2012.08.011, 2012.

1 **Evaluation of bacterial glycerol dialkyl glycerol tetraether and <sup>2</sup>H-**  
2 **<sup>18</sup>O biomarker proxies along a Central European topsoil transect**

3 Johannes Hepp<sup>1,2,\*</sup>, Imke K. Schäfer<sup>3</sup>, Verena Lanny<sup>4</sup>, Jörg Franke<sup>3</sup>, Marcel  
4 Bliedtner<sup>3,a</sup>, Kazimierz Rozanski<sup>5</sup>, Bruno Glaser<sup>2</sup>, Michael Zech<sup>2,6</sup>, Timothy I.  
5 Eglinton<sup>4</sup>, Roland Zech<sup>3,a</sup>

6 <sup>1</sup>Chair of Geomorphology and BayCEER, University of Bayreuth, 95440 Bayreuth, Germany and

7 <sup>2</sup>Institute of Agronomy and Nutritional Sciences, Soil Biogeochemistry, Martin-Luther-University  
8 Halle-Wittenberg, 06120 Halle, Germany

9 <sup>3</sup>Institute of Geography and Oeschger Centre for Climate Change Research, University of Bern, 3012  
10 Bern, Switzerland

11 <sup>4</sup>Department of Earth Science, ETH Zurich, 8092 Zurich, Switzerland

12 <sup>5</sup>Faculty of Physics and Applied Computer Science, AGH University of Science and Technology, 30-  
13 059 Kraków, Poland

14 <sup>6</sup>Institute of Geography, Faculty of Environmental Sciences, Technical University of Dresden, 01062  
15 Dresden, Germany

16 <sup>a</sup>now at Institute of Geography, Chair of Physical Geography, Friedrich-Schiller University of Jena,  
17 07743 Jena, Germany

18

19 \*corresponding author ([johannes-hepp@gmx.de](mailto:johannes-hepp@gmx.de))



20 **Keywords**

21 Leaf wax *n*-alkanes, hemicellulose sugars, pH, temperature, CBT, MBT', precipitation  $\delta^2\text{H}$  and  
22  $\delta^{18}\text{O}$ , relative humidity

23 **Abstract**

24 Molecular fossils, like bacterial branched glycerol dialkyl glycerol tetraethers (brGDGTs), and  
25 the stable isotopic composition of biomarkers, such as  $\delta^2\text{H}$  of leaf wax-derived *n*-alkanes ( $\delta^2\text{H}_{n\text{-alkane}}$   
26 alkane) or  $\delta^{18}\text{O}$  of hemicellulose-derived sugars ( $\delta^{18}\text{O}_{\text{sugar}}$ ) are increasingly used for the  
27 reconstruction of past climate and environmental conditions. Plant-derived  $\delta^2\text{H}_{n\text{-alkane}}$  and  
28  $\delta^{18}\text{O}_{\text{sugar}}$  values record the isotopic composition of plant source water ( $\delta^2\text{H}_{\text{source-water}}$  and  
29  $\delta^{18}\text{O}_{\text{source-water}}$ ), which usually reflects mean annual precipitation ( $\delta^2\text{H}_{\text{precipitation}}$  and  
30  $\delta^{18}\text{O}_{\text{precipitation}}$ ), modulated by evapotranspirative leaf water enrichment and biosynthetic  
31 fractionation. Accuracy and precision of respective proxies should be ideally evaluated at a  
32 regional scale. For this study, we analysed topsoils below coniferous and deciduous forests, as  
33 well as grassland soils along a Central European transect in order to investigate the variability  
34 and robustness of various proxies, and to identify effects related to vegetation. Soil pH-values  
35 derived from brGDGTs correlate reasonably well with measured soil pH-values, but  
36 systematically overestimate them ( $\Delta\text{pH} = 0.6 \pm 0.6$ ). The branched vs. isoprenoid tetraether  
37 index (BIT) can give some indication whether the pH reconstruction is reliable. Temperatures  
38 derived from brGDGTs overestimate mean annual air temperatures slightly ( $\Delta T_{\text{MA}} = 0.5^\circ\text{C}$   
39  $\pm 2.4$ ). Apparent isotopic fractionation ( $\epsilon_{n\text{-alkane/precipitation}}$  and  $\epsilon_{\text{sugar/precipitation}}$ ) is lower for  
40 grassland sites than for forest sites due to "signal damping", i.e. grass biomarkers do not record  
41 the full evapotranspirative leaf water enrichment. Coupling  $\delta^2\text{H}_{n\text{-alkane}}$  with  $\delta^{18}\text{O}_{\text{sugar}}$  allows to  
42 reconstruct the stable isotopic composition of the source water more accurately than without  
43 the coupled approach ( $\Delta\delta^2\text{H} = \sim -21\text{‰} \pm 22$  and  $\Delta\delta^{18}\text{O} = \sim -2.9\text{‰} \pm 2.8$ ). Similarly, relative  
44 humidity during daytime and vegetation period ( $\text{RH}_{\text{MDV}}$ ) can be reconstructed using the coupled  
45 isotope approach ( $\Delta\text{RH}_{\text{MDV}} = \sim -17 \pm 12$ ). Especially for coniferous sites, reconstructed  $\text{RH}_{\text{MDV}}$   
46 values as well as source water isotope composition underestimate the measured values. This  
47 can be likely explained by understory grass vegetation at the coniferous sites contributing  
48 significantly to the *n*-alkane pool but only marginally to the sugar pool in the topsoils.  
49 Furthermore, vegetation-dependent variable "signal damping" and  $\epsilon_{\text{bio}}$  along our European  
50 transect are difficult to quantify quantitatively but likely do contribute like microclimate  
51 variability to the rather large uncertainties in the source water isotope composition and RH  
52 reconstructions. Vegetation-related effects do, by contrast, likely not affect the brGDGT-  
53 derived reconstructions. Overall, GDGTs and the coupled  $\delta^2\text{H}_{n\text{-alkane}}\text{-}\delta^{18}\text{O}_{\text{sugar}}$  approach have  
54 great potential for more quantitative paleoclimate reconstructions.

**Gelöscht:** . The large uncertainty likely reflect the fact that biosynthetic fractionation is not constant, as well as microclimate variability.

## 58 **1 Introduction**

59 Information about the variability and consequences of past climate changes is a prerequisite for  
60 precise predictions regarding the present climate change. Molecular fossils, so called  
61 biomarkers, have great potential to enhance our understanding about variations of past climate  
62 and environmental changes. Lipid biomarkers in particular are increasingly used for  
63 paleoclimate and environmental reconstructions (e.g. Brincat et al., 2000; Eglinton and  
64 Eglinton, 2008; Rach et al., 2014; Romero-Viana et al., 2012; Schreuder et al., 2016). However  
65 strengths and limitations of respective proxies need to be known (Dang et al., 2016). For this,  
66 calibrations using modern reference samples are essential.

67 One famous and widely applied lipid biomarker group are terrestrial branched glycerol dialkyl  
68 glycerol tetraethers (brGDGTs). They are synthesized in the cell membranes of anaerobe  
69 heterotrophic soil bacteria (Oppermann et al., 2010; Weijers et al., 2010) have great potential  
70 for the reconstruction of past environmental conditions (e.g. Coffinet et al., 2017; Schreuder et  
71 al., 2016; Zech et al., 2012), although some uncertainties exist. Calibration studies suggest that  
72 the relative abundance of the individual brGDGTs varies with mean annual air temperature  
73 ( $T_{MA}$ ) and soil pH (Peterse et al., 2012; Weijers et al., 2007), at least across large, global climate  
74 gradients or along pronounced altitudinal gradients (Wang et al., 2017). However, in arid  
75 regions the production of brGDGT is limited, while isoprenoidal GDGTs (iGDGTs) produced  
76 by archaea provide the dominant part of the overall soil GDGT pool (Anderson et al., 2014;  
77 Dang et al., 2016; Dirghangi et al., 2013; Wang et al., 2013; Xie et al., 2012). The ratio of  
78 brGDGTs vs. isoprenoid GDGTs (BIT) can be used as indication whether a reconstruction of  
79  $T_{MA}$  and pH will be reliable. Moreover, Mueller-Niggemann et al. (2016) revealed an influence  
80 of the vegetation cover on the brGDGT producing soil microbes. From field experiments, it is  
81 known that vegetation type and mulching practice strongly effect soil temperature and moisture  
82 (Awe et al., 2015; Liu et al., 2014). Thus, multiple factors can be expected to influence soil  
83 microbial communities and GDGT production. So far, little is known about the variability of  
84 GDGT proxies on a regional scale, and a calibration study with small climate gradient but with  
85 different vegetation types might be useful.

86 Concerning paleohydrology proxies, compound specific stable hydrogen isotopes of leaf wax  
87 biomarkers, such as long chain *n*-alkanes ( $\delta^2H_{n\text{-alkanes}}$ ) record the isotopic signal of precipitation  
88 and therefore past climate and environmental conditions (Sachse et al., 2004, 2006). However,  
89 various influencing factors are known e.g. the moisture source to leaf waxes (Pedentchouk and  
90 Zhou, 2018 and Sachse et al., 2012 for review). Next is the evapotranspiration of leaf water  
91 (Feakins and Sessions, 2010; Kahmen et al., 2013; Zech et al., 2015), which is strongly driven  
92 by relative air humidity (RH; e.g. Cernusak et al., 2016 for review). In addition, a strong  
93 precipitation signal is known to be incorporated into long chain leaf waxes (Hou et al., 2008;  
94 Rao et al., 2009; Sachse et al., 2004). In paleoclimate studies, it is often not feasible to  
95 disentangle between the evapotranspirative enrichment from the precipitation signal. Zech et  
96 al. (2013) proposed to couple  $\delta^2H_{n\text{-alkane}}$  results with oxygen stable isotopes of hemicellulose-  
97 derived sugars ( $\delta^{18}O_{\text{sugar}}$ ). Assuming constant biosynthetic fractionation factors ( $\epsilon_{\text{bio}}$ ) for the  
98 different compound classes (*n*-alkanes and hemicellulose sugars), the coupling enables the  
99 reconstruction of the isotopic composition of leaf water, RH and  $\delta^2H$  and  $\delta^{18}O$  of plant source  
100 water ( $\approx \delta^2H$  and  $\delta^{18}O$  of precipitation; Tuthorn et al., 2015). So far, a detailed evaluation of

101 this approach on the European scale, as well as related effects concerning vegetation changes  
102 is missing.

103 We analysed topsoil samples under coniferous, deciduous and grassland vegetation along a  
104 Central European transect in order to estimate the variability of the biomarker proxies. More  
105 specifically, we aim to test whether:

106 (i) the vegetation type has an influence on the brGDGT proxies, the  $\delta^2\text{H}_{n\text{-alkane}}$  and the  $\delta^{18}\text{O}_{\text{sugar}}$   
107 stable isotopic composition, as well as on reconstructed  $\delta^2\text{H}_{\text{source-water}}$ ,  $\delta^{18}\text{O}_{\text{source-water}}$  and RH.

108 (ii) the published brGDGT proxies used for reconstructing mean annual temperature and soil  
109 pH are sensitive enough to reflect the medium changes in temperature and soil pH along our  
110 transect.

111 (iii) the coupled  $\delta^2\text{H}_{n\text{-alkane}}\text{-}\delta^{18}\text{O}_{\text{sugar}}$  approach enables a  $\delta^2\text{H}$  and  $\delta^{18}\text{O}$  of precipitation and RH  
112 reconstruction along the transect.

113

## 114 **2 Material and methods**

### 115 **2.1 Geographical setting and sampling**

116 In November 2012, we collected 29 topsoil samples (0-5 cm depth) from 16 locations along a  
117 transect from Southern Germany to Southern Sweden (Fig. 1A). We distinguished between sites  
118 with coniferous forest (con,  $n = 9$ ), deciduous forest (dec,  $n = 14$ ) and grassland (grass,  $n = 6$ )  
119 vegetation cover (for more details see Schäfer et al. (2016) and Tab. S1).

120

### 121 **2.2 Database of instrumental climate variables and isotope composition of precipitation**

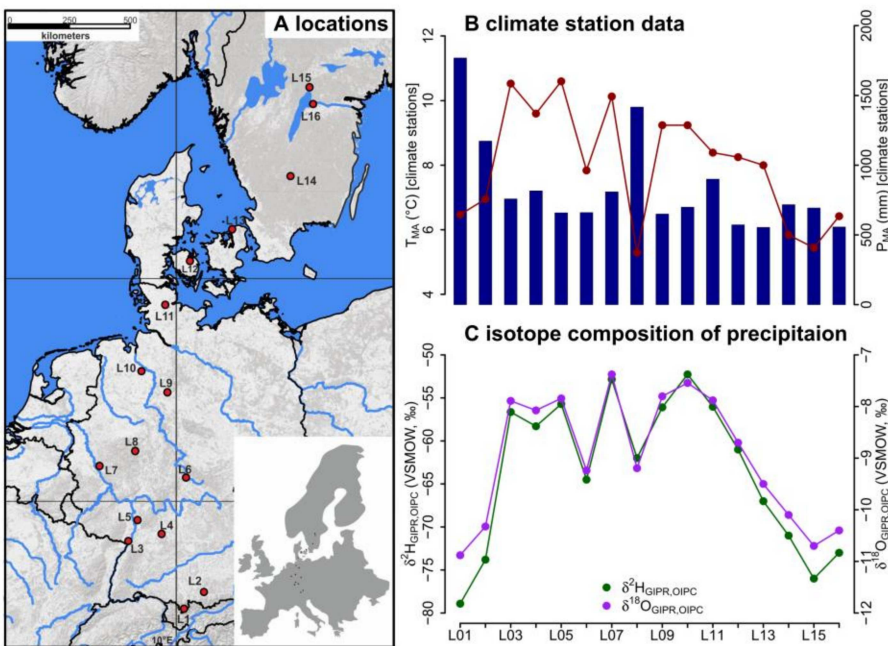
122 Climate data was derived from close-by weather observation stations operating by the regional  
123 institutions (Deutscher Wetterdienst (DWD) for Germany, Danmarks Meteorologiske Institut  
124 (DMI) for Denmark and the Sveriges Meteorologiska och Hydrologiska Institute (SMHI) for  
125 Sweden). The DWD provides hourly data for each station (DWD Climate Data Center, 2018b),  
126 enabling not only the calculation of  $T_{\text{MA}}$ , but also of the mean annual relative air humidity  
127 ( $\text{RH}_{\text{MA}}$ ), mean temperature and relative air humidity during the vegetation period ( $T$  and  
128  $\text{RH}_{\text{MV}}$ ), and of daytime temperature and relative humidity averages over the vegetation period  
129 ( $T$  and  $\text{RH}_{\text{MDV}}$ ). In addition, annual precipitation observations were used to derive the mean  
130 annual precipitation amount ( $P_{\text{MA}}$ ; DWD Climate Data Center, 2018b). From the DMI, the  
131 respective climate variables were derived from published technical reports (Cappelen, 2002;  
132 Frich et al., 1997; Laursen et al., 1999). The SMHI provides open data from which we derived  
133 the climate variables for the Swedish sites (Swedish Meteorological and Hydrological Institute,  
134 2018). For more details about the climate database used for calculations and comparisons, the  
135 reader is referred to Tab. S2.

136 For comprising German precipitation  $\delta^2\text{H}/\delta^{18}\text{O}$  along the transect, we realized a regionalisation  
137 (called  $\delta^2\text{H}_{\text{GIPR}}$  and  $\delta^{18}\text{O}_{\text{GIPR}}$ ) using online available data from 34 German GNIP stations, 4  
138 Austrian ANIP stations and the Groningen GNIP station (van Geldern et al., 2014;  
139 IAEA/WMO, 2018; Stumpp et al., 2014; Umweltbundesamt GmbH, 2018), following the  
140 approach of Schlotter (2007). However, instead of the multivariate regression procedure applied

141 by Schlotter (2007), we used a random forest approach (Hothorn et al., 2006; Strobl et al., 2007,  
 142 2008) to describe the relationship of squared latitude, latitude, longitude and altitude vs. long  
 143 term weighted means of precipitation  $\delta^2\text{H}$  and  $\delta^{18}\text{O}$ , and realized the prediction for each site  
 144 (see supplementary method description for more information). For the Danish and Swedish  
 145 sites, such a procedure was not possible. Hence, the annual precipitation  $\delta^2\text{H}$  and  $\delta^{18}\text{O}$  values  
 146 were derived from the Online Isotopes in Precipitation Calculator (OIPC, version 3.1), therefore  
 147 called  $\delta^2\text{H}_{\text{OIPC}}$  and  $\delta^{18}\text{O}_{\text{OIPC}}$  (Bowen, 2018; Bowen and Revenaugh, 2003; IAEA/WMO, 2015).  
 148 The finally used  $\delta^2\text{H}_{\text{GIPR,OIPC}}$  and  $\delta^{18}\text{O}_{\text{GIPR,OIPC}}$  data are given in Tab. S1.

149 The  $T_{\text{MA}}$  along the transect ranges from 5.3 to 10.6°C, and  $P_{\text{MA}}$  ranges from 554 to 1769 mm  
 150 (Fig. 1B). Precipitation  $\delta^2\text{H}/\delta^{18}\text{O}$  shows moderate changes along the transect,  $\delta^2\text{H}_{\text{GIPR,OIPC}}$   
 151 varies between -52 and -79‰, and  $\delta^{18}\text{O}_{\text{GIPR,OIPC}}$  ranges from -7.4 to -10.9‰ (Fig. 1C).

152 Correlations between  $\delta^{18}\text{O}_{\text{GIPR,OIPC}}$  and  $P_{\text{MA}}$ , altitude of the locations,  $T_{\text{MA}}$  are given in the  
 153 supplementary material (Fig. S1 to S3), along with a  $\delta^2\text{H}_{\text{GIPR,OIPC}}$  vs.  $\delta^{18}\text{O}_{\text{GIPR,OIPC}}$  scatter plot  
 154 (Fig. S4).



155 **Fig. 1.** (A) Sample locations (red dots, map source: US National Park Service), (B) variations  
 156 of mean annual air temperature ( $T_{\text{MA}}$ , red dots and line) and mean annual precipitation ( $P_{\text{MA}}$ ,  
 157 blue bars) derived from close-by climate station data, and (C) hydrogen and oxygen stable  
 158 isotope composition of precipitation ( $\delta^2\text{H}_{\text{GIPR,OIPC}}$  and  $\delta^{18}\text{O}_{\text{GIPR,OIPC}}$ , respectively) as derived for  
 159 the sampled transect locations (see section 2.2 GIPR  $\delta^2\text{H}$  and  $\delta^{18}\text{O}$  generation procedure). The  
 160 reader is referred to section 2.2 (and Tab. S1 and S2) for database and reference information of  
 161 data plotted in (B) and (C).

163

164 **2.3 Soil extractions and analysis**

165 2.3.1 GDGTs and pH

166 A detailed description of sample preparation for lipid analysis can be found in Schäfer et al.  
167 (2016). Briefly, 1–6 g freeze-dried and grounded soil sample was microwave extracted with 15  
168 ml dichloromethane (DCM)/methanol (MeOH) 9:1 (v:v) at 100°C for 1 h. Extracts were  
169 separated over aminopropyl silica gel (Supelco, 45 µm) pipette columns. The nonpolar fraction  
170 (including *n*-alkanes) was eluted with hexane and further purified over AgNO<sub>3</sub> coated silica  
171 pipette columns (Supelco, 60–200 mesh) and zeolite (Geokleen Ltd.). The GDGT-containing  
172 fraction was eluted with DCM:MeOH 1:1 (v:v), re-dissolved in hexane/isopropanol (IPA) 99:1  
173 (v:v) and transferred over 0.45 µm PTFE filters into 300 µl inserts. For quantification, a known  
174 amount of a C<sub>46</sub> diol standard was added after transfer. The samples were analysed at ETH  
175 Zurich using an Agilent 1260 Infinity series HPLC–atmospheric chemical pressure ionization  
176 mass spectrometer (HPLC–APCI-MS) equipped with a Grace Prevail Cyano column (150 mm  
177 × 2.1 mm; 3 µm). The GDGTs were eluted isocratically with 90% A and 10% B for 5 min and  
178 then with a linear gradient to 18% B for 34 min at 0.2 ml min<sup>-1</sup>, where A=hexane and  
179 B=hexane/isopropanol (9:1, v:v). Injection volume was 10 µl and single ion monitoring of  
180 [M+H]<sup>+</sup> was used to detect GDGTs.

181 The pH of the samples was measured in the laboratory of the Soil Biogeochemistry group,  
182 Institute of Agronomy and Nutritional Sciences, Martin-Luther-University Halle-Wittenberg,  
183 using a pH meter in a 1:3 soil:water (w/v) mixture.

184

185 2.3.2 δ<sup>2</sup>H<sub>*n*-alkane</sub>

186 The hydrogen isotopic composition of the highest concentrated *n*-alkanes (*n*-C<sub>25</sub>, *n*-C<sub>27</sub>, *n*-C<sub>29</sub>,  
187 *n*-C<sub>31</sub>, and *n*-C<sub>33</sub>) was determined using a TRACE GC Ultra Gas Chromatography connected to  
188 a Delta V Plus Isotope Ratio Mass Spectrometer via a <sup>2</sup>H pyrolysis reactor kept at 1420 °C (GC-  
189 <sup>2</sup>H-Py-IRMS; Thermo Scientific, Bremen, Germany) at ETH Zurich (Christoph et al., 2019).  
190 For more details about *n*-alkane quantification the reader is referred to Schäfer et al. (2016).  
191 The compound-specific <sup>2</sup>H/<sup>1</sup>H ratios were calibrated against an external standard with C<sub>15</sub>–C<sub>35</sub>  
192 homologues. External standard mixtures (A4 mix from A. Schimmelmann, University of  
193 Indiana) were run between the samples for multipoint linear normalization. The H<sup>+</sup><sub>3</sub> factor was  
194 determined on each measurement day and was constant throughout the periods of the sample  
195 batches. Samples were analysed in duplicates, and results typically agreed within 4% (average  
196 difference = 1.4%). All δ<sup>2</sup>H values are expressed relative to the Vienna Standard Mean Ocean  
197 Water (V-SMOW).

198

199 2.3.3 δ<sup>18</sup>O<sub>sugar</sub>

200 Hemicellulose sugars were extracted and purified using a slightly modified standard procedure  
201 (Amelung et al., 1996; Guggenberger et al., 1994; Zech and Glaser, 2009). Briefly, myoinositol  
202 was added to the samples prior to extraction as first internal standard. The sugars were released  
203 hydrolytically using 4M trifluoroacetic acid for 4 h at 105°C, cleaned over glass fiber filters and  
204 further purified using XAD and Dowex columns. Before derivatization with methylboronic acid  
205 (Knapp, 1979), the samples were frozen, freeze-dried, and 3-O-methylglucose in dry pyridine

206 was added as second internal standard. Compound-specific hemicellulose sugar  $^{18}\text{O}$   
 207 measurements were performed in the laboratory of the Soil Biogeochemistry group, Institute of  
 208 Agronomy and Nutritional Sciences, Martin-Luther-University Halle-Wittenberg, using GC-  
 209  $^{18}\text{O}$ -Py-IRMS (all devices from Thermo Fisher Scientific, Bremen, Germany). Standard  
 210 deviations of the triplicate measurements were 1.4‰ (over 29 investigated samples) for  
 211 arabinose and xylose, respectively. We focus on these two hemicellulose-derived neutral sugars  
 212 arabinose and xylose as they strongly predominate over fucose in terrestrial plants, soils and  
 213 sediments (Hepp et al., 2016 and references therein). Rhamnose concentrations were too low to  
 214 obtain reliable  $\delta^{18}\text{O}$  results. All  $\delta^{18}\text{O}$  values are expressed relative to the Vienna Standard Mean  
 215 Ocean Water (V-SMOW).

216

## 217 2.4 Theory and Calculations

### 218 2.4.1 Calculations used for the GDGT-based reconstructions

219 The branched and isoprenoid tetraether (BIT) index is calculated according to Hopmans et al.  
 220 (2004), for structures see Fig. S5:

$$221 \text{ BIT} = \frac{\text{Ia} + \text{IIa} + \text{IIIa}}{\text{Ia} + \text{IIa} + \text{IIIa} + \text{crenarchaeol}} \quad (1)$$

222 The cyclopentane moiety number of brGDGTs correlates negatively with soil pH (Weijers et  
 223 al., 2007), which led to the development of the cyclization of branched tetraethers (CBT) ratio.  
 224 CBT and the CBT based pH ( $\text{pH}_{\text{CBT}}$ ) were calculated according to Peterse et al. (2012):

$$225 \text{ CBT} = -\log \frac{\text{Ib} + \text{IIb}}{\text{Ia} + \text{IIa}}, \quad (2)$$

$$226 \text{ pH}_{\text{CBT}} = 7.9 - 1.97 \times \text{CBT}. \quad (3)$$

227 The number of methyl groups in brGDGTs correlates negatively with  $T_{\text{MA}}$  and soil pH (Peterse  
 228 et al., 2012; Weijers et al., 2007). Thus, the ratio of the methylation of branched tetraethers  
 229 (MBT) ratio and the CBT ratio can be used to reconstruct  $T_{\text{MA}}$ . We use the equation given by  
 230 Peterse et al. (2012):

$$231 \text{ MBT}' = \frac{\text{Ia} + \text{Ib} + \text{Ic}}{\text{Ia} + \text{Ib} + \text{Ic} + \text{IIa} + \text{IIb} + \text{IIc} + \text{IIIa}}, \quad (4)$$

$$232 T_{\text{MA}} = 0.81 - 5.67 \times \text{CBT} + 31.0 \times \text{MBT}'. \quad (5)$$

233

### 234 2.4.2 Calculations and concepts used for the coupled $\delta^2\text{H}$ - $\delta^{18}\text{O}$ approach

235 The apparent fractionation is calculated according to Cernusak et al. (2016):

$$236 \varepsilon_{n\text{-alkane/precipitation}} = \left( \frac{\delta^2\text{H}_{n\text{-alkane}} - \delta^2\text{H}_{\text{GIPR,OIPC}}}{1 + \delta^2\text{H}_{\text{GIPR,OIPC}}/1000} \right), \quad (6)$$

$$237 \varepsilon_{\text{sugar/precipitation}} = \left( \frac{\delta^{18}\text{O}_{\text{sugar}} - \delta^{18}\text{O}_{\text{GIPR,OIPC}}}{1 + \delta^{18}\text{O}_{\text{GIPR,OIPC}}/1000} \right). \quad (7)$$

238 The isotopic composition of leaf water ( $\delta^2\text{H}_{\text{leaf-water}}$  and  $\delta^{18}\text{O}_{\text{leaf-water}}$ ) can be calculated using  $\varepsilon_{\text{bio}}$   
 239 for  $\delta^2\text{H}_{n\text{-alkane}}$  (-160‰, Sachse et al., 2012; Sessions et al., 1999) and  $\delta^{18}\text{O}_{\text{sugar}}$  (+27‰, Cernusak  
 240 et al., 2003; Schmidt et al., 2001):

$$241 \delta^2\text{H}_{\text{leaf-water}} = \left( \frac{1000 + \delta^2\text{H}_{n\text{-alkane}}}{1000 + \varepsilon_{\text{bio}}(n\text{-alkane})} \right) \times 10^3 - 1000, \quad (8)$$

242 
$$\delta^{18}\text{O}_{\text{leaf-water}} = \left( \frac{1000 + \delta^{18}\text{O}_{\text{sugar}}}{1000 + \epsilon_{\text{bio}}(\text{sugar})} \right) \times 10^3 - 1000. \quad (9)$$

243 Zech et al. (2013) introduced the conceptual model for the coupled  $\delta^2\text{H}_{n\text{-alkane}}\text{-}\delta^{18}\text{O}_{\text{sugar}}$  approach  
 244 in detail. Briefly, the coupled approach is based on the following assumptions (illustrated in  
 245 Fig. 8): (i) The isotopic composition of precipitation, which is set to be equal to the plant source  
 246 water, typically plots along the global meteoric water line (GMWL;  $\delta^2\text{H} = 8 \times \delta^{18}\text{O} + 10$ ) in a  
 247  $\delta^{18}\text{O}$  vs.  $\delta^2\text{H}$  space (Craig, 1961); (ii) Source water uptake by plants does not lead to any  
 248 fractionation (e.g. Dawson et al., 2002), and significant evaporation of soil water can be  
 249 excluded; (iii) Evapotranspiration leads to enrichment of the remaining leaf water along the  
 250 local evaporation line (LEL; Allison et al., 1985; Bariac et al., 1994; Walker and Brunel, 1990),  
 251 compared to the source water taken up by the plant; (iv) The biosynthetic fractionation is  
 252 assumed to be constant. In addition, isotopic equilibrium between plant source water (~  
 253 weighted mean annual precipitation) and the local atmospheric water vapour is assumed.  
 254 Further assumption concerns the isotope steady-state in the evaporating leaf water reservoir.  
 255 The coupled approach allows for reconstructing the isotopic composition of plant source water  
 256 ( $\delta^2\text{H}_{\text{source-water}}$  and  $\delta^{18}\text{O}_{\text{source-water}}$ ) from the reconstructed leaf water, by calculating the intercepts  
 257 of the LELs with the GMWL (Zech et al., 2013). The slope of the LEL ( $S_{\text{LEL}}$ ) can be assessed  
 258 by the following equation (Gat, 1971):

259 
$$S_{\text{LEL}} = \frac{\epsilon_2^* + C_k^2}{\epsilon_{18}^* + C_k^{18}}, \quad (10)$$

260 where  $\epsilon^*$  are equilibrium isotope fractionation factors and  $C_k$  are kinetic fractionation factors.  
 261 The latter equals to 25.1‰ and 28.5‰, for  $C_k^2$  and  $C_k^{18}$ , respectively (Merlivat, 1978). The  
 262 equilibrium fractionation factors can be derived from empirical equations (Horita and  
 263 Wesolowski, 1994) by using  $T_{\text{MDV}}$  values. For two Danish sites  $T_{\text{MDV}}$  are not available, instead  
 264  $T_{\text{MV}}$  is used here (section 2.2 and Tab. S2).

265 In a  $\delta^{18}\text{O}\text{-}\delta^2\text{H}$  diagram, the distance of the leaf water from the GMWL define the deuterium-  
 266 excess of leaf water ( $d_{\text{leaf-water}} = \delta^2\text{H}_{\text{leaf-water}} - 8 \times \delta^{18}\text{O}_{\text{leaf-water}}$ , according Dansgaard, (1964); Fig.  
 267 8). To convert  $d_{\text{leaf-water}}$  into mean RH during daytime and vegetation period ( $\text{RH}_{\text{MDV}}$ ), a  
 268 simplified Craig-Gordon model can be applied (Zech et al., 2013):

269 
$$\text{RH} = 1 - \frac{\Delta d}{\epsilon_2^* - 8 \times \epsilon_{18}^* + C_k^2 - 8 \times C_k^{18}}, \quad (11)$$

270 where  $\Delta d$  is the difference in  $d_{\text{leaf-water}}$  and the deuterium-excess of source water ( $d_{\text{source-water}}$ ).

271

## 272 2.5 Statistics

273 In the statistical analysis we checked sample distributions for normality (Shapiro and Wilk,  
 274 1965) and for equal variance (Levene, 1960). If normality and equal variances are given, we  
 275 perform an Analysis of Variance (ANOVA). If that is not the case, we conduct the non-  
 276 parametric Kruskal-Wallis Test. ANOVA or Kruskal-Wallis are used to find significant  
 277 differences ( $\alpha=0.05$ ) between the vegetation types (deciduous, conifer and grass).

278 In order to describe the relation along a 1:1 line, the coefficient of correlation ( $R^2$ ) was  
 279 calculated as  $R^2 = 1 - \frac{\sum(\text{modeled} - \text{measured})^2}{\sum(\text{measured} - \text{measured mean})^2}$ . The small  
 280  $r^2$  is taken as coefficient of correlation of a linear regression between a dependent (y) and

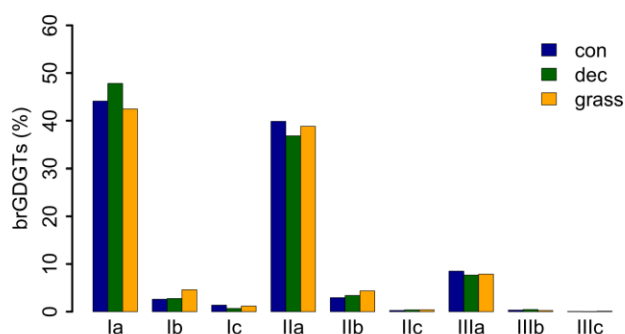
281 explanatory variable(s). The root mean square error (RMSE) of the relationships was calculated  
 282 as  $RMSE = \sqrt{\left(\frac{1}{n} \cdot \sum(\text{modeled} - \text{measured})^2\right)}$ . All data plotting and statistical analysis was  
 283 realized in R (version 3.2.2; R Core Team, 2015).

284

## 285 3 Results and Discussion

### 286 3.1 GDGT concentrations

287 GDGT Ia has the highest concentration under all vegetation types, followed by GDGT IIa and  
 288 GDGT IIIa (Fig. 2). GDGT Ib, IIb and Ic occur in minor, GDGT IIc and IIIb only in trace  
 289 amounts. GDGT IIIc was below the detection limit in most of the samples (Tab. S3). Although  
 290 other studies document an influence of the vegetation cover on soil temperature and soil water  
 291 content, which control the microbial community composition in soils (Awe et al., 2015; Liu et  
 292 al., 2014; Mueller-Niggemann et al., 2016), we find no statistically different pattern of the  
 293 individual brGDGTs.



294

295 **Fig. 2.** Mean concentrations of individual brGDGTs as percentage of all brGDGTs for the three  
 296 investigated types. Abbreviations: con = coniferous forest sites (n=9); dec = deciduous forest  
 297 sites (n=14); grass = grassland sites (n=6).

298 Total concentrations of brGDGTs range from 0.32 to 9.17  $\mu\text{g/g}$  dry weight and tend to be  
 299 highest for the coniferous samples and lowest for the grasses (Fig. 3A, Tab. S3). Bulk brGDGT  
 300 concentrations lie within the range of other studies examining soils of mid latitude regions  
 301 (Huguet et al., 2010b, 2010a; Weijers et al., 2011). Similar concentrations in coniferous and  
 302 deciduous samples imply that brGDGT production does not strongly vary in soils below  
 303 different forest types. The grass samples show lower brGDGT concentrations compared to the  
 304 forest samples, but this is probably mainly due to ploughing of the grass sites in former times  
 305 and hence admixing of mineral subsoil material. The differences in brGDGT concentrations are  
 306 not significant ( $p\text{-value} = 0.06$ ).

307

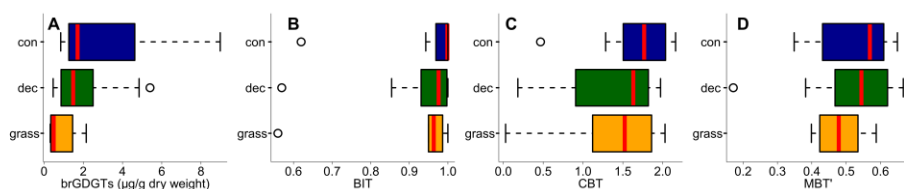
### 308 3.2 BIT index

309 Most of the samples have a BIT index higher than 0.9 (Fig 3B and Tab. S3). The BIT-values  
 310 are typical for soils in humid and temperate climate regions (Weijers et al., 2006). However,



311 outliers exist. The most likely source of iGDGTs in soils are Thaumarchaeota, i.e. aerobic  
 312 ammonia oxidizing archaea producing Crenarchaeol and its regioisomer (Schouten et al., 2013  
 313 and references therein), when precipitation amount drops below 700-800 mm (Dang et al.,  
 314 2016; Dirghangi et al., 2013). The  $P_{MA}$  data of our sampling sites mostly show precipitation >  
 315 550 mm (Fig. 1B), but one has to be aware that this data is based on the climate station nearest  
 316 to the respective sampling locations and microclimate effects, such as sunlight exposure,  
 317 canopy cover or exposition might have a pronounced influence on the brGDGT vs. iGDGT  
 318 distribution. Mueller-Niggemann et al. (2016) found higher BIT indices in upland soils  
 319 compared to paddy soils and stated that the management type also influences BIT values in  
 320 soils. Along our transect, grass sites tend to have slightly lower BIT-values than forest sites,  
 321 probably due to the absence of a litter layer and hence, no isolation mechanism preventing  
 322 evaporation of soil water. Differences between vegetation types are not significant (p-value =  
 323 0.32).

Gelöscht: s



324 **Fig. 3.** (A) Total concentrations of brGDGTs in  $\mu\text{g g}^{-1}$  dry weight, as well as (B) BIT, (C) CBT  
 325 and (D) MBT'. Abbreviations: con = coniferous forest sites (n=9); dec = deciduous forest sites  
 326 (n=14); grass = grassland sites (n=6). Box plots show median (red line), interquartile range  
 327 (IQR) with upper (75%) and lower (25%) quartiles, lowest whisker still within 1.5IQR of lower  
 328 quartile, and highest whisker still within 1.5IQR of upper quartile, dots mark outliers.

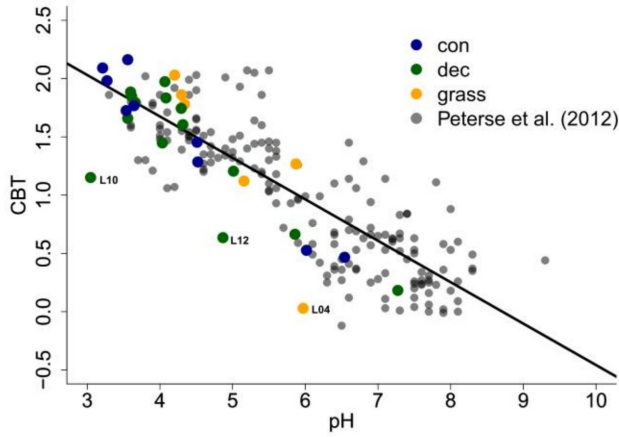
330

### 331 3.3 CBT-derived pH

332 The CBT ratio shows a pronounced variation independent of vegetation type with values  
 333 between 0.03 and 2.16 (Fig 3C). The coniferous samples tend to be highest, but the differences  
 334 between vegetation types are not significant (p-value = 0.48). The CBT index can be related to  
 335 pH in acidic and/or humid soils (e.g. Dirghangi et al., 2013; Mueller-Niggemann et al., 2016;  
 336 Peterse et al., 2012; Weijers et al., 2007) but might be an indicator of soil water content and  
 337 hence, precipitation in more arid and alkaline soils (e.g. Dang et al., 2016). There is a  
 338 pronounced correlation between CBT and soil pH (Fig. 4), which is in good agreement with  
 339 other studies from mid latitude regions where precipitation is relatively high (Anderson et al.,  
 340 2014 and references therein). Moreover, the CBT to pH relationship in terms of slope and  
 341 intersect in our dataset ( $\text{CBT} = -0.47 \times \text{pH} + 3.5$ ,  $r^2 = 0.7$ , p-value < 0.0001, n = 29) is well  
 342 comparable to the correlation described for the global calibration dataset of Peterse et al. (2012)  
 343 ( $\text{CBT} = -0.36 \times \text{pH} + 3.1$ ,  $r^2 = 0.7$ , p-value < 0.0001, n = 176).

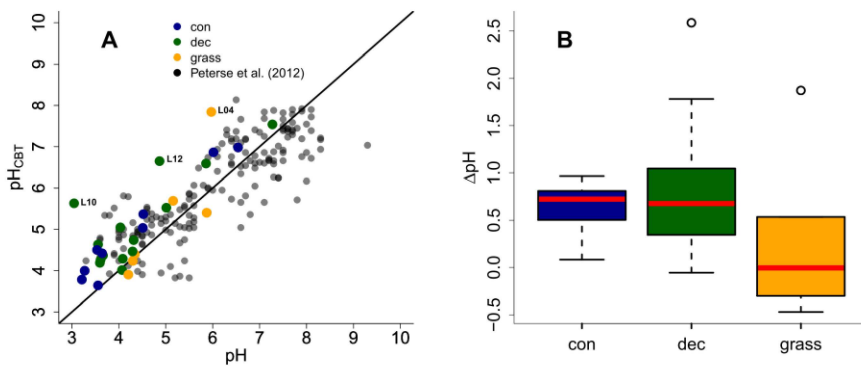
344 However, there are some outliers in the CBT-pH correlation, which need a further examination  
 345 (see locations grass L04, dec L10 and dec L12 as marked in Figs. 4 and 5). The outliers show  
 346 lower BIT indices (< 0.85, Tab. S3). Even though the data from the nearest climate station  
 347 suggest no abnormal  $P_{MA}$ . Local effects such as differences in the amount of sunlight exposure,  
 348 nutrient availability for brGDGT producing organisms or, most likely soil water content might

350 influence the brGDGT production at these locations (Anderson et al., 2014; Dang et al., 2016).  
 351 A lower BIT index as well as a lower CBT occur when soil water content decreases (Dang et  
 352 al., 2016; Sun et al., 2016) or when aeration is high and less anoxic microhabitats for GDGT  
 353 producing microbes exist (e.g. Dirghangi et al., 2013).



354  
 355 **Fig. 4.** CBT to pH relationship in our dataset in comparison to the global calibration dataset  
 356 from Peterse et al. (2012) ( $CBT = -0.36 \times pH + 3.1$ ,  $r^2 = 0.7$ ,  $p\text{-value} < 0.0001$ ,  $n = 176$ , black  
 357 line). Abbreviations: con = coniferous forest sites ( $n=9$ ); dec = deciduous forest sites ( $n=14$ );  
 358 grass = grassland sites ( $n=6$ ).

359  
 360 As the CBT and pH are similarly correlated in our dataset and the global dataset of Peterse et  
 361 al. (2012), the CBT-derived pH correlated well with the actual pH (Fig. 5A;  $R^2 = 0.3$ ).  
 362 Expressed as  $\Delta pH$  (CBT-derived pH - measured pH), there is a tendency that the GDGTs result  
 363 in an overestimation of the real pH for the forest sites (Fig. B). Yet a Kruskal-Wallis test shows  
 364 no statistically significant difference between the vegetation types, with a p-value of 0.13. The  
 365 overall  $\Delta pH$  of  $0.6 \pm 0.6$  shows that the reconstruction of soil pH using brGDGTs works well  
 366 along this transect.



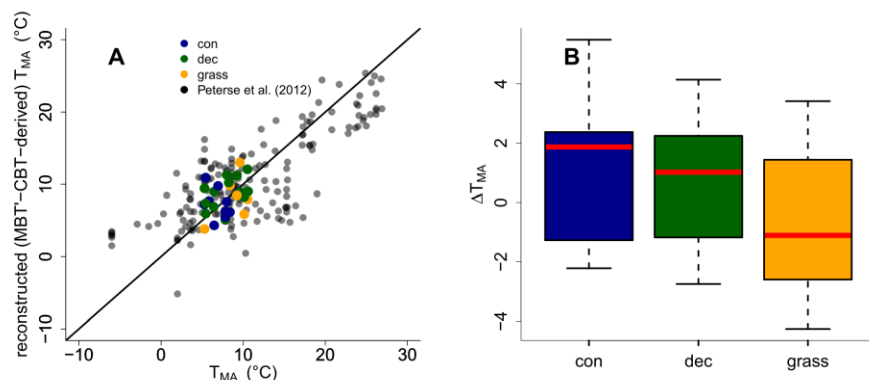
367

368 **Fig. 5.** (A) Correlation between measured pH and reconstructed soil pH ( $pH_{CBT}$ ) from our  
 369 transect data in comparison to the global calibration dataset from Peterse et al. (2012) ( $R^2 = 0.7$ ,  
 370  $RMSE = 0.75$ ,  $n = 176$ ). Black line indicates the 1:1 relationship. (B) Boxplots of  $\Delta pH$  (refers  
 371 to  $pH_{CBT}-pH$ ). Box plots show median (red line), interquartile range (IQR) with upper (75%)  
 372 and lower (25%) quartiles, lowest whisker still within 1.5IQR of lower quartile, and highest  
 373 whisker still within 1.5IQR of upper quartile, dots mark outliers. Abbreviations: con =  
 374 coniferous forest sites ( $n=9$ ); dec = deciduous forest sites ( $n=14$ ); grass = grassland sites ( $n=6$ ).

375

### 376 3.4 MBT'-CBT-derived $T_{MA}$ reconstructions

377 The MBT' shows high variability with values ranging from 0.17 to 0.67 no statistical  
 378 differences between vegetation types ( $p$ -value = 0.54; Fig. 3D, Tab. S3). When comparing  
 379 reconstructed (MBT'-CBT-derived)  $T_{MA}$  with climate station  $T_{MA}$ , the data plot close to the 1:1  
 380 line, and fit well into the global dataset of Peterse et al. (2012) (Fig. 6A). The  $\Delta T_{MA}$  reveal an  
 381 overall offset of  $0.5^\circ C \pm 2.4$  and there is no statistically difference between vegetation types  
 382 (Fig. 6B). The standard deviation in  $\Delta T_{MA}$  of  $\pm 2.4$  is well in line with the RMSE of 5.0 for the  
 383 global calibration dataset (Peterse et al., 2012).



384 **Fig. 6.** (A) Correlation between climate station  $T_{MA}$  and reconstructed (MBT'-CBT-derived)  
 385  $T_{MA}$ . For comparison, the global calibration dataset from Peterse et al. (2012) is shown. The  
 386 black line indicates the 1:1 relationship. (B) Boxplots of  $\Delta T_{MA}$  (refers to reconstructed  $T_{MA}$ -  
 387  $T_{MA}$  from climate stations) in the different vegetation types from our transect study. Box plots  
 388 show median (red line), interquartile range (IQR) with upper (75%) and lower (25%) quartiles,  
 389 lowest whisker still within 1.5IQR of lower quartile, and highest whisker still within 1.5IQR of  
 390 upper quartile, dots mark outliers. Abbreviations: con = coniferous forest sites ( $n=9$ ); dec =  
 391 deciduous forest sites ( $n=14$ ); grass = grassland sites ( $n=6$ ).

392

### 394 3.5 Potential impact of the used liquid chromatography method on pH and $T_{MA}$ 395 reconstructions

396 The GDGT data presented in this study are not acquired on the up-to-date method (e.g. compare  
 397 De Jonge et al., 2014 vs. Zech et al., 2012c). De Jonge et al. (2014) presented a new liquid  
 398 chromatography method which enables the separation for the brGDGTs with  $m/z$  1036, 1034

399 and 1032, 1050, 1048 and 1046 into 6-methyl and 5-methyl stereoisomers. The old method did  
400 not allow such a separation (Zech et al., 2012c), thus in the calibration often the sum of 6 and  
401 5-methylated brGDGTs was used (see and compare De Jonge et al., 2014 vs. Peterse et al., 2012).  
402 This introduces scatter to the MBT'-CBT-based  $T_{MA}$  reconstructions and can cause a correlation  
403 between pH and MBT' (for more details see De Jonge et al., 2014). De Jonge et al. (2014)  
404 moreover show that the 6-methyl brGDGTs are ubiquitous abundant in soils from all over the  
405 world, based on reanalysing the dataset of Peterse et al. (2012). However, they also compare  
406 reconstructed  $T_{MA}$  values based MBT'-CBT calibration (Peterse et al., 2012) and their new  
407 developed  $T_{MA}$  calibration and state that they plot around a 1:1 line. They furthermore state,  
408 that especially for arid areas larger deviations can be expected. Finally, they conclude that the  
409 use of the new developed calibrations will improve the  $T_{MA}$  and pH reconstructions for areas  
410 with arid climate conditions. Because our study transect spans from southern Germany to  
411 southern Sweden, representing temperate and humid climate conditions, we argue that the usage  
412 of the older liquid chromatography method do not introduce a systematic error in our  $T_{MA}$  and  
413 pH reconstructions. Still, a higher variability/scatter could be associated with the calibration of  
414 Peterse et al. (2012) and therefore also present in our  $T_{MA}$  and pH reconstructions.

415

### 416 **3.6 Apparent fractionation of $\delta^2H$ and $\delta^{18}O$ in the different vegetation types**

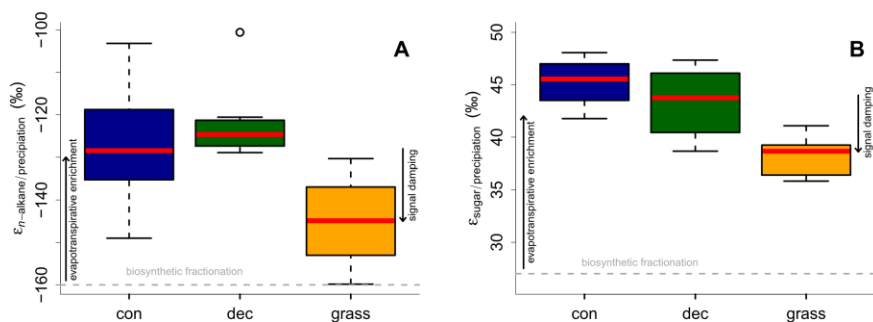
417 The  $\delta^2H$  values could be obtained for *n*-alkanes  $C_{27}$ ,  $C_{29}$  and  $C_{31}$  in all samples and additionally  
418 at two locations for *n*- $C_{25}$  and *n*- $C_{33}$  at six other locations. The  $\delta^2H_{n-alkane}$  values, calculated as  
419 mean of *n*- $C_{25}$  to *n*- $C_{31}$   $\delta^2H$ , ranges from -156 to -216‰. Pooled standard deviations show an  
420 overall average of 3.6‰. The  $\delta^{18}O_{sugar}$  values, calculated as the area weighted means for  
421 arabinose and xylose, ranges from 27.7 to 39.4‰. The average weighted mean standard  
422 deviation is 1.4‰. The compound-specific isotope data is summarized along with the  
423 calculations in Tab. S4.

424 Apparent fractionation ( $\epsilon_{n-alkane/precipitation}$ ) is on the order of -120 to -150‰, i.e. a bit less than  
425 the biosynthetic fraction of -160‰. This implies that evapotranspirative enrichment is ~ 10 to  
426 40‰ (Fig. 7A).  $\epsilon_{n-alkane/precipitation}$  is lower for grass sites compared to the forest sites. Differences  
427 are significant between deciduous and grass sites (p-value = 0.005). This finding supports the  
428 results of other studies (Kahmen et al., 2013; Liu and Yang, 2008; McInerney et al., 2011), and  
429 can be named "signal damping". Grasses do not only incorporate the evaporatively-enriched  
430 leaf water only but also unenriched xylem water in the growth and differentiation zone of  
431 grasses (Gamarra et al., 2016; Liu et al., 2017).

432 The grass-derived hemicellulose sugar biomarkers do not fully record the evapotranspirative  
433 enrichment of the leaf water, either, as indicated by lower apparent fractionation ( $\epsilon_{sugar/precipitation}$ )  
434 in Fig. 7B. The differences are significant between forest and grass sites (p-value < 0.005). This  
435 is in agreement with a study on cellulose extracted from grass blades (Helliker and Ehleringer,  
436 2002), and again, the "signal damping" can be explained with incorporation of enriched leaf  
437 water and non-enriched stem water.

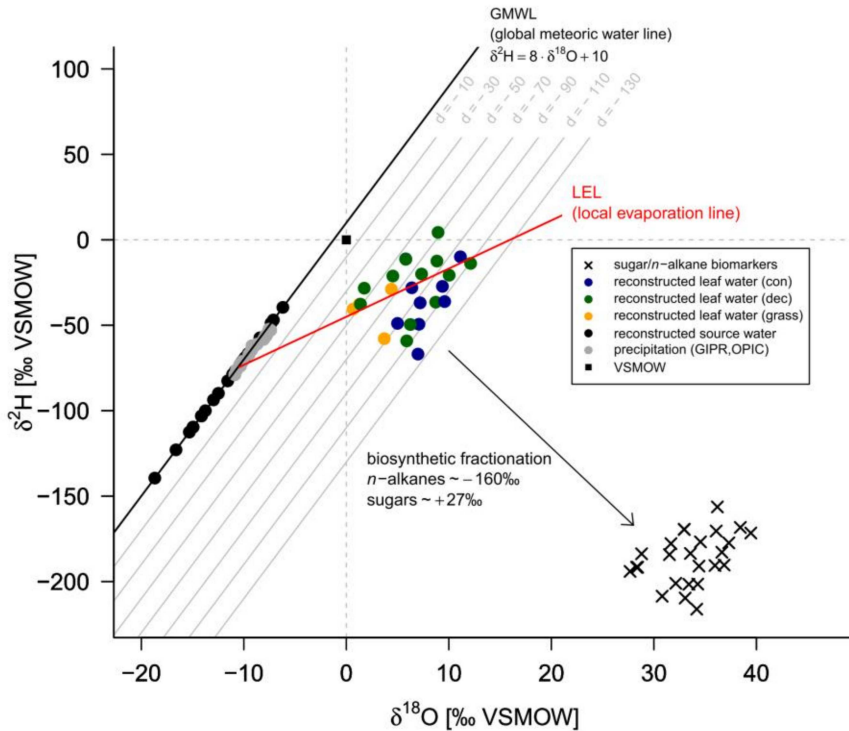
438 Based on the comparison of evapotranspirative enrichment between forest and grass sites, the  
439 "signal damping" can be quantified to be ~ 31% for the hemicellulose sugars, and ~ 49% for  
440 the *n*-alkanes. This is in agreement with other studies that reported a loss of 22% of the leaf

441 water enrichment for hemicellulose sugars (Helliker and Ehleringer, 2002) and 39 to 62% loss  
 442 of the leaf water enrichment for *n*-alkanes (Gamarra et al., 2016).



443  
 444 **Fig. 7.** Apparent fractionation (A)  $\epsilon_{n\text{-alkane/precipitation}}$  and (B)  $\epsilon_{\text{sugar/precipitation}}$ . Biosynthetic  
 445 fractionation factors according to section 2.4.2. Box plots show median (red line), interquartile  
 446 range (IQR) with upper (75%) and lower (25%) quartiles, lowest whisker still within 1.5IQR  
 447 of lower quartile, and highest whisker still within 1.5IQR of upper quartile, dots mark outliers.  
 448 Abbreviations: con = coniferous forest sites (n=9); dec = deciduous forest sites (n=11 and 14  
 449 for *n*-alkanes and sugars, respectively); grass = grassland sites (n=4 and 6 for *n*-alkanes and  
 450 sugars, respectively). The figure conceptually illustrates the effect of biosynthetic fractionation  
 451 and evapotranspirative enrichment as well as “signal damping”.

452  
 453 **3.7  $\delta^2\text{H}_{\text{source-water}}$  and  $\delta^{18}\text{O}_{\text{source-water}}$  reconstructions**  
 454 The  $\delta^2\text{H}$  versus  $\delta^{18}\text{O}$  diagram shown in Fig. 8 graphically illustrates the reconstruction of  $\delta^2\text{H}_{\text{leaf-}}$   
 455 water and  $\delta^{18}\text{O}_{\text{leaf-water}}$  (colored dots) from  $\delta^2\text{H}_{n\text{-alkane}}$  and  $\delta^{18}\text{O}_{\text{sugar}}$  (crosses), as well as the  
 456 reconstruction of  $\delta^2\text{H}_{\text{source-water}}$  and  $\delta^{18}\text{O}_{\text{source-water}}$  (black dots). For reconstructing  $\delta^2\text{H}_{\text{source-water}}$   
 457 and  $\delta^{18}\text{O}_{\text{source-water}}$ , LELs with an average slope of  $2.8 \pm 0.1$  (Eq. 10) can be generated through  
 458 every leaf water point and the intercepts of these LELs with the GMWL.



459  
 460 **Fig. 8.**  $\delta^2\text{H}$  vs.  $\delta^{18}\text{O}$  diagram illustrating the coupled  $\delta^2\text{H}_{n\text{-alkane}}\text{-}\delta^{18}\text{O}_{\text{sugar}}$  approach: measured  
 461  $\delta^2\text{H}_{n\text{-alkane}}$  and  $\delta^{18}\text{O}_{\text{sugar}}$  values, reconstructed  $\delta^2\text{H}_{\text{leaf-water}}$  and  $\delta^{18}\text{O}_{\text{leaf-water}}$  (according Eqs. 8 and  
 462 9) and reconstructed  $\delta^2\text{H}_{\text{source-water}}$  and  $\delta^{18}\text{O}_{\text{source-water}}$  in comparison to GIPR and OIPC-based  
 463  $\delta^2\text{H}_{\text{precipitation}}$  and  $\delta^{18}\text{O}_{\text{precipitation}}$ . Abbreviations: con = coniferous forest sites (n=9); dec =  
 464 deciduous forest sites (n=11); grass = grassland sites (n=4).

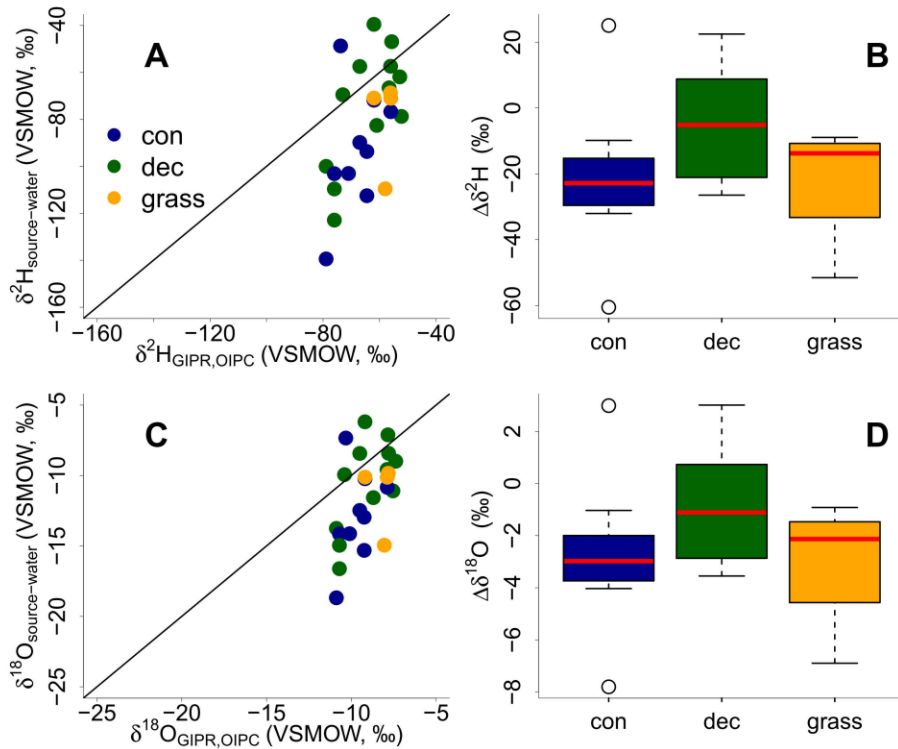
465  
 466 The reconstructed  $\delta^2\text{H}_{\text{source-water}}$  and  $\delta^{18}\text{O}_{\text{source-water}}$  results can be compared with the  $\delta^2\text{H}_{\text{GIPR,OIPC}}$   
 467 and  $\delta^{18}\text{O}_{\text{GIPR,OIPC}}$  data (Fig. 9). This comparison reveals that the coupled  $\delta^2\text{H}_{n\text{-alkane}}\text{-}\delta^{18}\text{O}_{\text{sugar}}$   
 468 approach yields more accurate  $\delta^2\text{H}_{\text{source-water}}$  and  $\delta^{18}\text{O}_{\text{source-water}}$  compared to single  $\delta^2\text{H}_{n\text{-alkane}}$   
 469 approaches. However, the range of the reconstructed  $\delta^2\text{H}_{\text{source-water}}$  and  $\delta^{18}\text{O}_{\text{source-water}}$  values is  
 470 clearly larger than in  $\delta^2\text{H}_{\text{GIPR,OIPC}}$  and  $\delta^{18}\text{O}_{\text{GIPR,OIPC}}$  values.  $\delta^2\text{H}$  is systematically underestimated  
 471 by  $\sim 21\text{‰} \pm 22$  (Fig. 9B) and  $\delta^{18}\text{O}$  by  $\sim 2.9\text{‰} \pm 2.8$  (Fig. 9D). The type of vegetation seems to  
 472 be not particularly relevant (p-value = 0.18 for  $\Delta\delta^2\text{H}$  and p-value = 0.34 for  $\Delta\delta^{18}\text{O}$ ).  
 473 Nevertheless, the systematic offsets tend to be lowest for the deciduous sites ( $\Delta\delta^2\text{H}$  and  $\Delta\delta^{18}\text{O}$  is  
 474 closer to zero with  $\sim -5\text{‰} \pm 15$  and  $\sim -1.1\text{‰} \pm 2.1$ ), followed by grass sites ( $\sim -14\text{‰} \pm 20$  and  $\sim$   
 475  $2.1\text{‰} \pm 2.6$ ). In comparison, the coniferous sites show the largest offsets ( $\sim -23\text{‰} \pm 26$  for  $\Delta\delta^2\text{H}$   
 476  $\sim -3.0\text{‰} \pm 3.3$  for  $\Delta\delta^{18}\text{O}$ ). Differences are, however, not statistically significant. The systematic  
 477 offset and the large variability might have more specific reasons, and we suggest that this is  
 478 related to the type of vegetation. Deciduous trees produce lots of leaf waxes and sugars (e.g.  
 479 Prietzel et al., 2013; Zech et al., 2012a), and all biomarkers reflect and record the

480 evapotranspirative enrichment of the leaf water (e.g. Kahmen et al., 2013; Tuthorn et al., 2014).  
481 However, coniferous trees produce quite low amounts of *n*-alkanes (Diefendorf and Freimuth,  
482 2016; Zech et al., 2012a), while sugar concentrations are as high as in other vascular plants (e.g.  
483 Hepp et al., 2016; Prietzel et al., 2013). For the coniferous soil samples this means that the *n*-  
484 alkanes stem most likely from the understory whereas the sugars originate from grasses and  
485 coniferous needles. When the understory is dominated by grass species then the *n*-alkane  
486 biomarkers do not record the full leaf water enrichment signal, whereas the sugars from the  
487 needles do. The reconstructed leaf water for the coniferous sites is therefore too negative  
488 concerning  $\delta^2\text{H}$ , and reconstructed  $\delta^2\text{H}_{\text{source-water}}$  and  $\delta^{18}\text{O}_{\text{source-water}}$  values thus also become too  
489 negative (Fig. 8). Concerning the grass sites the following explanation can be found. Correcting  
490 for “signal damping” makes the reconstructed leaf water points more positive and shifts them  
491 in Fig. 8 up and right. As the “signal damping” is stronger for  $\delta^2\text{H}$  than for  $\delta^{18}\text{O}$  the corrected  
492 leaf water points would now be above the uncorrected ones. The corrected leaf water points leads  
493 to more positive reconstructed  $\delta^2\text{H}_{\text{source-water}}$  and  $\delta^{18}\text{O}_{\text{source-water}}$  values for the grass sites.  
494 However, Gao et al. (2014) and Liu et al. (2016) showed that the  $\epsilon_{\text{bio}}$  of monocotyledon plants  
495 could be larger than those of dicotyledonous ones. This would therefore cause a more negative  
496 apparent fractionation factor for grasses compared to trees. We observe that the apparent  
497 fractionation is indeed more negative for the grass sites compared to the forest sites. The effects  
498 of “signal damping” vs. variable  $\epsilon_{\text{bio}}$  along with vegetation types are indistinguishable here. As  
499 an outlook for a future study, we therefore strongly recommend a comparison between the here  
500 measured  $\delta^2\text{H}_{n\text{-alkane}}$  values with modelled ones using a new available model approach from  
501 Konecny et al. (2019), which could provide insights if such vegetation effects on  $\epsilon_{\text{bio}}$  of  $^2\text{H}$  in  
502 *n*-alkanes are describable.

503

504 Vegetation type specific rooting depths could partly cause the overall high variability in  
505 reconstructed  $\delta^2\text{H}_{\text{source-water}}$  and  $\delta^{18}\text{O}_{\text{source-water}}$ . Deep rooting species most likely use the water  
506 from deeper soil horizons and/or shallow ground water, which is equal to the (weighted) mean  
507 annual precipitation (e.g. Herrmann et al., 1987). Shallow rooting plants take up water from  
508 upper soil horizons, which is influenced by seasonal variations in  $\delta^2\text{H}_{\text{precipitation}}$  and  $\delta^{18}\text{O}_{\text{precipitation}}$   
509 and by soil water enrichment (Dubbert et al., 2013). Thus, the overall assumption that the source  
510 water of the plants reflects the local (weighted) mean precipitation might be not fully valid for  
511 all sites. Moreover, a partly contribution of root-derived rather than leaf-derived sugar  
512 biomarkers in our topsoil samples is very likely. This does, by contrast, not apply for *n*-alkanes,  
513 which are hardly produced in roots (Zech et al., 2012b and the discussion therein).





514  
 515 **Fig. 9.** Correlation of reconstructed  $\delta^2\text{H}_{\text{source-water}}$  and  $\delta^{18}\text{O}_{\text{source-water}}$  vs. precipitation  $\delta^2\text{H}_{\text{GIPR,OIPC}}$   
 516 and  $\delta^{18}\text{O}_{\text{GIPR,OIPC}}$  (A and C). Black lines indicate 1:1 relationship. Differences between  
 517 reconstructed source water and precipitation ( $\Delta\delta^2\text{H}, \Delta\delta^{18}\text{O} = \delta^2\text{H}_{\text{source-water}}, \delta^{18}\text{O}_{\text{source-water}} -$   
 518  $\delta^2\text{H}_{\text{GIPR,OIPC}}, \delta^{18}\text{O}_{\text{GIPR,OIPC}}$ ) for the three different vegetation types (B and D). Box plots show  
 519 median (red line), interquartile range (IQR) with upper (75%) and lower (25%) quartiles, lowest  
 520 whisker still within 1.5IQR of lower quartile, and highest whisker still within 1.5IQR of upper  
 521 quartile. Abbreviations: con = coniferous forest sites (n=9); dec = deciduous forest sites (n=11);  
 522 grass = grassland sites (n=4).

523 Moreover, the high variability within the vegetation types could be caused by variability in  $\epsilon_{\text{bio}}$   
 524 of  $^2\text{H}$  in *n*-alkanes, as well as  $^{18}\text{O}$  in sugars. There is an ongoing discussion about the correct  
 525  $\epsilon_{\text{bio}}$  for  $^{18}\text{O}$  in hemicellulose sugars (Sternberg, 2014 vs. Zech et al., 2014), and  $\epsilon_{\text{bio}}$  is probably  
 526 not constant over all vegetation types. This translates into errors concerning leaf water  
 527 reconstruction and thus for reconstructing  $\delta^2\text{H}_{\text{source-water}}$  and  $\delta^{18}\text{O}_{\text{source-water}}$  values (Eq. 9 and Fig.  
 528 8). Likewise, the  $\epsilon_{\text{bio}}$  values reported in the literature for  $^2\text{H}$  of *n*-alkanes can be off from -160‰  
 529 by tens of permille (Feakins and Sessions, 2010; Tipple et al., 2015; Feakins et al., 2016;  
 530 Freimuth et al., 2017). The degree to which hydrogen originates from NADPH rather than leaf  
 531 water is important, because NADPH is more negative (Schmidt et al., 2003). The wide range  
 532 in biosynthetic  $^2\text{H}$  fractionation factors, which can be even larger, is therefore also related to  
 533 the carbon and energy metabolism state of plants (Cormier et al., 2018).

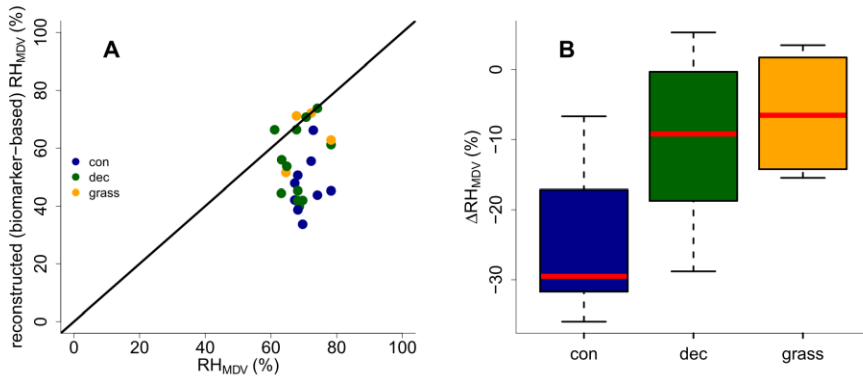


534 **3.8 RH reconstruction**

535 Reconstructed  $RH_{MDV}$  ranges from 34 to 74%, while  $RH_{MDV}$  from climate station data range  
536 from 61 to 78% (Fig. 10A). Biomarker-based values thus systematically underestimate the  
537 station data ( $\Delta RH_{MDV} = -17\% \pm 12$ ). Yet the offsets are much less for deciduous tree and grass  
538 sites ( $\Delta RH_{MDV} = -10\% \pm 12$  and  $-7\% \pm 9$ , respectively; Fig. 10B). The offsets for the coniferous  
539 sites are  $-30\% \pm 11$ , and significantly larger than for the deciduous and grass sites ( $p$ -values  $<$   
540  $0.05$ ).

541 Too low reconstructed  $RH_{MDV}$  values for the coniferous sites make sense in view of the  
542 previously discussed option that soils contain  $n$ -alkanes from the understory (which is  
543 dominated by grass species), while sugars stem from needles and grasses. As explained earlier  
544 already, the “signal damping” leads to too negative reconstructed  $\delta^2H_{leaf-water}$  (whereas  $\delta^{18}O$  is  
545 affected less by the “signal damping”), and too negative  $\delta^2H_{leaf-water}$  translates into  
546 overestimated  $d$ -excess and underestimated RH values. In Fig. 8, a correction for this require  
547 moving the coniferous leaf water data points upwards towards more positive  $\delta^2H$  values, thus  
548 the distance between the leaf water and the source water is reduced. It should be noted that also  
549 here variable  $\epsilon_{bio}$  along with vegetation types could not be distinguished from “signal damping”  
550 effects.

551 The underestimation of RH for the deciduous and grass sites could be partly associated with the  
552 use of the GMWL as baseline for the coupled  $\delta^2H_{n-alkane}-\delta^{18}O_{sugar}$  approach. The deuterium-  
553 excess of the LMWLs is generally lower than the  $+10\text{‰}$  of the GMWL, while the slopes of the  
554 LMWLs are well comparable to the GMWL (Stumpp et al., 2014). In addition, if soil water  
555 evaporation occurred before water uptake by the plants, this would lead to an underestimation  
556 of biomarker-based  $RH_{MDV}$  values. It can be furthermore assumed that plant metabolism is  
557 highest during times with direct sunshine and high irradiation, i.e. during noon at sunny days.  
558 The relevant RH could therefore be lower than the climate station-derived  $RH_{MDV}$ . Indeed,  
559 already climate station  $RH_{MDV}$  is considerable lower than  $RH_{MA}$  and  $RH_{MV}$  (Tab. S1).



560  
561 **Fig. 10.** (A) Comparison of reconstructed (biomarker-based)  $RH_{MDV}$  values and climate station  
562  $RH_{MDV}$  data. The black line indicates the 1:1 relationship. (B) Differences between  
563 reconstructed and climate station  $RH_{MDV}$  values ( $\Delta RH_{MDV} = \text{reconstructed} - \text{climate station}$   
564  $RH_{MDV}$ ) for the three different vegetation types along the transect. Abbreviations: con =  
565 coniferous forest sites (n=9); dec = deciduous forest sites (n=11); grass = grassland sites (n=4).

566 The uncertainty of reconstructed  $RH_{MDV}$  values are large for all three investigated vegetation  
567 types, and again these uncertainties are probably also related to  $\epsilon_{bio}$ , which is most likely not  
568 constant as assumed for our calculations. Moreover, microclimate variability is underestimated  
569 in our approach. As mentioned in sections 2.4.2 and 3.7, in the coupled approach not only the  
570 source water of the plants is equated with (weighted) mean annual precipitation, but also an  
571 isotopic equilibrium between the source water and the (local) atmospheric water vapour is  
572 assumed. However, in areas with distinct seasonality this might be not fully valid. To account  
573 for this lack of equilibrium between precipitation and local atmospheric water vapour, apparent  
574  $\epsilon$  values can be calculated with data from Jacob and Sonntag, (1991). As shown by Hepp et al.  
575 (2018) those values can be used to achieve alternative RH reconstructions based on the coupled  
576  $\delta^2H_{n\text{-alkane}}-\delta^{18}O_{\text{sugar}}$  approach. Such calculated  $RH_{MDV}$  values are on average 1.5% more  
577 negative than the original values. However, this difference in RH is far below the analytical  
578 uncertainties of the compound-specific biomarker isotope analysis.

579 Finally, the integration time of the investigated topsoils has to be discussed. Unfortunately, no  
580  $^{14}C$  dates are available for the soil samples. However, most likely the organic matter has been  
581 built up over a longer timescale than the available climate data, which is used for comparison.  
582 In combination with vegetation changes/management changes throughout that period, this  
583 could surely lead to a less tight relationship of the reconstructions compared to the climate  
584 station data. Root input of arabinose and xylose seems to be of minor relevance in our topsoil  
585 samples. Otherwise, the reconstructed  $\delta^{18}O_{\text{sugar}}$  values would be too negative resulting in  
586  $RH_{MDV}$  overestimations, which is not observed.

587

## 588 4 Conclusions

589 We were able to show that

- 590 (i) the vegetation type does not significantly influence the brGDGT concentrations and  
591 proxies, yet the coniferous sites tend to have higher brGDGT concentrations, BIT  
592 indices and CBT-MBT' ratios, while grass sites tend to be lowest.
- 593 (ii) CBT faithfully records soil pH with a median  $\Delta pH$  of  $0.6 \pm 0.6$ , The CBT  
594 overestimates the real pH particularly at the forest sites.
- 595 (iii) CBT-MBT'-derived  $T_{MA}$  reflect the climate station-derived  $T_{MA}$  values with a  
596 median  $\Delta T_{MA}$  of  $0.5^\circ C \pm 2.4$ , but again slightly too high reconstruction for the forest  
597 sites were observed.
- 598 (iv) differences in the apparent fractionation between the investigated vegetation types  
599 could be caused by "signal damping" or variable  $\epsilon_{bio}$ , which are indistinguishable  
600 here.
- 601 (v) the reconstructed  $\delta^2H_{\text{source-water}}$  and  $\delta^{18}O_{\text{source-water}}$  reflect the  $\delta^2H_{GIPR,OIPC}$  and  
602  $\delta^{18}O_{GIPR,OIPC}$  with a systematic offset for  $\delta^2H$  of  $\sim -21\% \pm 22$  and for  $\delta^{18}O$  of  $\sim -2.9\% \pm 2.8$   
603 (based on overall medians of  $\Delta\delta^2H$ ,  $\delta^{18}O$ ). This is caused by too negative  
604 reconstructions for coniferous and grass sites. For coniferous sites, this can be  
605 explained with *n*-alkanes originating from understory grasses. As for the grass sites,  
606 the "signal damping" or variable  $\epsilon_{bio}$  along with vegetation types more effect  $\delta^2H$

Gelöscht: along with vegetation types

Gelöscht: s

609 than  $\delta^{18}\text{O}$ . This leads to too negative reconstructed  $\delta^2\text{H}_{\text{leaf-water}}$  values and thus to too  
610 negative  $\delta^2\text{H}_{\text{source-water}}$  and  $\delta^{18}\text{O}_{\text{source-water}}$  reconstructions.  
611 (vi) reconstructed (biomarker-based)  $\text{RH}_{\text{MDV}}$  values tend to underestimate climate  
612 station-derived  $\text{RH}_{\text{MDV}}$  values ( $\Delta\text{RH}_{\text{MDV}} = \sim -17\% \pm 12$ ). For coniferous sites the  
613 underestimations are strongest, which can be explained with understory grasses  
614 being the main source of  $n$ -alkanes for the investigated soils under coniferous  
615 forests.

616 Overall, our study highlights the great potential of GDGTs and the coupled  $\delta^2\text{H}_{n\text{-alkane}}\text{-}\delta^{18}\text{O}_{\text{sugar}}$   
617 approach for more quantitative paleoclimate reconstructions. Taking into account effects of  
618 different vegetation types improves correlations and reconstructions. This holds particularly  
619 true for the coupled  $\delta^2\text{H}_{n\text{-alkane}}\text{-}\delta^{18}\text{O}_{\text{sugar}}$  approach, which is affected by “signal damping” of the  
620 grass vegetation or variable  $\varepsilon_{\text{bio}}$  along with vegetation types. By contrast, vegetation-related  
621 effects do not strongly influence the brGDGT-derived reconstructions. Assuming constant  
622 biosynthetic fractionation is likely a considerable source of uncertainty and should be in focus  
623 in future field and/or modelling studies. Climate chamber experiments would be very useful to  
624 further evaluate and refine the coupled  $\delta^2\text{H}_{n\text{-alkane}}\text{-}\delta^{18}\text{O}_{\text{sugar}}$  approach, because uncertainties  
625 related to microclimate variability can be reduced. Field experiments like ours suffer from the  
626 fact that biomarker pools in the sampled topsoils may have been affected by past vegetation  
627 and climate changes and by the rather small range covered by the sampled transect. Both makes  
628 the comparison between reconstructions and observations more difficult compared to large  
629 datasets und well defined conditions.

630

## 631 Acknowledgements

632 We thank L. Wüthrich, H. Veit, T. Sprafke, A. Groos (all University of Bern), A. Kühnel  
633 (Technical University of Munich) for constructive discussions and statistical advices, and M.  
634 Schaarschmidt (University of Bayreuth), C. Heinrich and M. Benesch (Martin-Luther-  
635 University Halle-Wittenberg) for laboratory assistance during  $\delta^{18}\text{O}_{\text{sugar}}$  analysis and pH  
636 measurements, respectively. The Swiss National Science Foundation (PP00P2 150590) funded  
637 this research. J. Hepp greatly acknowledges the support by the German Federal Environmental  
638 Foundation (DBU) in form of his PhD-fellowship.

639

## 640 References

- 641 Allison, G. B., Gat, J. R. and Leaney, F. W. J.: The relationship between deuterium and oxygen-  
642  $^{18}$  delta values in leaf water, *Chemical Geology*, 58, 145–156, 1985.
- 643 Amelung, W., Cheshire, M. V. and Guggenberger, G.: Determination of neutral and acidic  
644 sugars in soil by capillary gas-liquid chromatography after trifluoroacetic acid hydrolysis,  
645 *Soil Biology and Biochemistry*, 28(12), 1631–1639, 1996.
- 646 Anderson, V. J., Shanahan, T. M., Saylor, J. E., Horton, B. K. and Mora, A. R.: Sources of local  
647 and regional variability in the MBT/CBT paleotemperature proxy: Insights from a  
648 modern elevation transect across the Eastern Cordillera of Colombia, *Organic*  
649 *Geochemistry*, 69, 42–51, doi:10.1016/j.orggeochem.2014.01.022, 2014.

- 650 Awe, G. O., Reichert, J. M. and Wendroth, O. O.: Temporal variability and covariance  
651 structures of soil temperature in a sugarcane field under different management practices  
652 in southern Brazil, *Soil and Tillage Research*, 150, 93–106,  
653 doi:10.1016/j.still.2015.01.013, 2015.
- 654 Bariac, T., Gonzalez-Dunia, J., Katerji, N., Béthenod, O., Bertolini, J. M. and Mariotti, A.:  
655 Spatial variation of the isotopic composition of water ( $^{18}\text{O}$ ,  $^2\text{H}$ ) in the soil-plant-  
656 atmosphere system, 2. Assessment under field conditions, *Chemical Geology*, 115, 317–  
657 333, 1994.
- 658 Bowen, G. J.: The Online Isotopes in Precipitation Calculator, version 3.1., 2018.
- 659 Bowen, G. J. and Revenaugh, J.: Interpolating the isotopic composition of modern meteoric  
660 precipitation, *Water Resources Research*, 39(10), 1–13, doi:10.1029/2003WR002086,  
661 2003.
- 662 Brincat, D., Yamada, K., Ishiwatari, R., Uemura, H. and Naraoka, H.: Molecular-isotopic  
663 stratigraphy of long-chain *n*-alkanes in Lake Baikal Holocene and glacial age sediments,  
664 *Organic Geochemistry*, 31(4), 287–294, doi:10.1016/S0146-6380(99)00164-3, 2000.
- 665 Cappelen, J.: Danish Climatological Normals 1971-2000 - for selected stations., 2002.
- 666 Cernusak, L. A., Wong, S. C. and Farquhar, G. D.: Oxygen isotope composition of phloem sap  
667 in relation to leaf water in *Ricinus communis*, *Functional Plant Biology*, 30(10), 1059–  
668 1070, 2003.
- 669 Cernusak, L. A., Barbour, M. M., Arndt, S. K., Cheesman, A. W., English, N. B., Feild, T. S.,  
670 Helliker, B. R., Holloway-Phillips, M. M., Holtum, J. A. M., Kahmen, A., Mcinerney, F.  
671 A., Munksgaard, N. C., Simonin, K. A., Song, X., Stuart-Williams, H., West, J. B. and  
672 Farquhar, G. D.: Stable isotopes in leaf water of terrestrial plants, *Plant Cell and  
673 Environment*, 39(5), 1087–1102, doi:10.1111/pce.12703, 2016.
- 674 Christoph, H., Eglinton, T. I., Zech, W., Sosin, P. and Zech, R.: A 250 ka leaf-wax  $\delta\text{D}$  record  
675 from a loess section in Darai Kalon, Southern Tajikistan, *Quaternary Science Reviews*,  
676 208, 118–128, doi:10.1016/j.quascirev.2019.01.019, 2019.
- 677 Coffinet, S., Huguet, A., Anquetil, C., Derenne, S., Pedentchouk, N., Bergonzini, L.,  
678 Omuombo, C., Williamson, D., Jones, M., Majule, A. and Wagner, T.: Evaluation of  
679 branched GDGTs and leaf wax *n*-alkane  $\delta^2\text{H}$  as (paleo) environmental proxies in East  
680 Africa, *Geochimica et Cosmochimica Acta*, 198, 182–193,  
681 doi:10.1016/j.gca.2016.11.020, 2017.
- 682 Cormier, M.-A., Werner, R. A., Sauer, P. E., Gröcke, D. R., M.C., L., Wieloch, T., Schleucher,  
683 J. and Kahmen, A.:  $^2\text{H}$  fractionations during the biosynthesis of carbohydrates and lipids  
684 imprint a metabolic signal on the  $\delta^2\text{H}$  values of plant organic compounds, *New  
685 Phytologist*, 218(2), 479–491, doi:10.1111/nph.15016, 2018.
- 686 Craig, H.: Isotopic Variations in Meteoric Waters, *Science*, 133, 1702–1703, 1961.
- 687 Dang, X., Yang, H., Naafs, B. D. A., Pancost, R. D. and Xie, S.: Evidence of moisture control  
688 on the methylation of branched glycerol dialkyl glycerol tetraethers in semi-arid and arid  
689 soils, *Geochimica et Cosmochimica Acta*, 189, 24–36, doi:10.1016/j.gca.2016.06.004,  
690 2016.
- 691 Dansgaard, W.: Stable isotopes in precipitation, *Tellus*, 16(4), 436–468, doi:10.1111/j.2153-  
692 3490.1964.tb00181.x, 1964.

- 693 Dawson, T. E., Mambelli, S., Plamboeck, A. H., Templer, P. H. and Tu, K. P.: Stable Isotopes  
694 in Plant Ecology, *Annual Review of Ecology and Systematics*, 33(1), 507–559,  
695 doi:10.1146/annurev.ecolsys.33.020602.095451, 2002.
- 696 Diefendorf, A. F. and Freimuth, E. J.: Extracting the most from terrestrial plant-derived *n*-alkyl  
697 lipids and their carbon isotopes from the sedimentary record: A review, *Organic*  
698 *Geochemistry*, 103(January), 1–21, doi:10.1016/j.orggeochem.2016.10.016, 2016.
- 699 Dirghangi, S. S., Pagani, M., Hren, M. T. and Tipple, B. J.: Distribution of glycerol dialkyl  
700 glycerol tetraethers in soils from two environmental transects in the USA, *Organic*  
701 *Geochemistry*, 59, 49–60, doi:10.1016/j.orggeochem.2013.03.009, 2013.
- 702 Dubbert, M., Cuntz, M., Piayda, A., Maguás, C. and Werner, C.: Partitioning evapotranspiration  
703 - Testing the Craig and Gordon model with field measurements of oxygen isotope ratios  
704 of evaporative fluxes, *Journal of Hydrology*, 496, 142–153,  
705 doi:10.1016/j.jhydrol.2013.05.033, 2013.
- 706 DWD Climate Data Center: Historical annual precipitation observations for Germany. [online]  
707 Available from: [ftp://ftp-](ftp://ftp-cdc.dwd.de/pub/CDC/observations_germany/climate/hourly/precipitation/historical/)  
708 [cdc.dwd.de/pub/CDC/observations\\_germany/climate/hourly/precipitation/historical/](ftp://ftp-cdc.dwd.de/pub/CDC/observations_germany/climate/hourly/precipitation/historical/)  
709 (Accessed 20 September 2018a), 2018.
- 710 DWD Climate Data Center: Historical hourly station observations of 2m air temperature and  
711 humidity for Germany. [online] Available from: [ftp://ftp-](ftp://ftp-cdc.dwd.de/pub/CDC/observations_germany/climate/hourly/air_temperature/historical/)  
712 [cdc.dwd.de/pub/CDC/observations\\_germany/climate/hourly/air\\_temperature/historical/](ftp://ftp-cdc.dwd.de/pub/CDC/observations_germany/climate/hourly/air_temperature/historical/)  
713 (Accessed 19 September 2018b), 2018.
- 714 Eglinton, T. I. and Eglinton, G.: Molecular proxies for paleoclimatology, *Earth and Planetary*  
715 *Science Letters*, 275(1), 1–16, 2008.
- 716 Feakins, S. J. and Sessions, A. L.: Controls on the D/H ratios of plant leaf waxes in an arid  
717 ecosystem, *Geochimica et Cosmochimica Acta*, 74(7), 2128–2141,  
718 doi:<http://dx.doi.org/10.1016/j.gca.2010.01.016>, 2010.
- 719 Feakins, S. J., Bentley, L. P., Salinas, N., Shenkin, A., Blonder, B., Goldsmith, G. R., Ponton,  
720 C., Arvin, L. J., Wu, M. S., Peters, T., West, A. J., Martin, R. E., Enquist, B. J., Asner, G.  
721 P. and Malhi, Y.: Plant leaf wax biomarkers capture gradients in hydrogen isotopes of  
722 precipitation from the Andes and Amazon, *Geochimica et Cosmochimica Acta*, 182, 155–  
723 172, doi:10.1016/j.gca.2016.03.018, 2016.
- 724 Freimuth, E. J., Diefendorf, A. F. and Lowell, T. V.: Hydrogen isotopes of *n*-alkanes and *n*-  
725 alkanolic acids as tracers of precipitation in a temperate forest and implications for  
726 paleorecords, *Geochimica et Cosmochimica Acta*, 206, 166–183,  
727 doi:10.1016/j.gca.2017.02.027, 2017.
- 728 Frich, P., Rosenørn, S., Madsen, H. and Jensen, J. J.: Observed Precipitation in Denmark, 1961-  
729 90., 1997.
- 730 Gamarra, B., Sachse, D. and Kahmen, A.: Effects of leaf water evaporative <sup>2</sup>H-enrichment and  
731 biosynthetic fractionation on leaf wax *n*-alkane δ<sup>2</sup>H values in C3 and C4 grasses, *Plant,*  
732 *Cell and Environment Environment*, 39, 2390–2403, doi:10.1111/pce.12789, 2016.
- 733 Gat, J. R.: Comments on the Stable Isotope Method in Regional Groundwater Investigations,  
734 *Water Resources Research*, 7(4), 980–993, doi:10.1029/WR007i004p00980, 1971.
- 735 van Geldern, R., Baier, A., Subert, H. L., Kowol, S., Balk, L. and Barth, J. A. C.: (Table S1)

736 Stable isotope composition of precipitation sampled at Erlangen, Germany between 2010  
737 and 2013 for station GeoZentrum located at Erlangen city center, in In supplement to: van  
738 Geldern, R et al. (2014): Pleistocene paleo-groundwater as a pristine fresh water resource  
739 in southern Germany – evidence from stable and radiogenic isotopes. *Science of the Total*  
740 *Environment*, 496, 107-115, <https://doi.org/10.1016/j.scitotenv.2014.05.012>, PANGAEA., 2014.

741 Guggenberger, G., Christensen, B. T. and Zech, W.: Land-use effects on the composition of  
742 organic matter in particle-size separates of soil: I. Lignin and carbohydrate signature,  
743 *European Journal of Soil Science*, 45(December), 449–458, 1994.

744 Helliker, B. R. and Ehleringer, J. R.: Grass blades as tree rings: environmentally induced  
745 changes in the oxygen isotope ratio of cellulose along the length of grass blades, *New*  
746 *Phytologist*, 155, 417–424, 2002.

747 Hepp, J., Rabus, M., Anhäuser, T., Bromm, T., Laforsch, C., Sirocko, F., Glaser, B. and Zech,  
748 M.: A sugar biomarker proxy for assessing terrestrial versus aquatic sedimentary input,  
749 *Organic Geochemistry*, 98, 98–104, doi:10.1016/j.orggeochem.2016.05.012, 2016.

750 Hepp, J., Wüthrich, L., Bromm, T., Bliedtner, M., Schäfer, I. K., Glaser, B., Rozanski, K.,  
751 Sirocko, F., Zech, R. and Zech, M.: How dry was the Younger Dryas? Evidence from a  
752 coupled  $\delta^2\text{H}$ - $\delta^{18}\text{O}$  biomarker paleohygrometer, applied to the Lake Gemündener Maar  
753 sediments, Western Eifel, Germany, *Climate of the Past Discussions*, (September), 1–44,  
754 doi:10.5194/cp-2018-114, 2018.

755 Herrmann, A., Maloszewski, P. and Stichler, W.: Changes of  $^{18}\text{O}$  contents of precipitation water  
756 during seepage in the unsaturated zone, in *Proceedings of International Symposium on*  
757 *Groundwater Monitoring and Management*, 23 - 28 March, p. 22, Institut of Water  
758 *Management Berlin (GDR) with support of UNESCO, Dresden.*, 1987.

759 Hopmans, E. C., Weijers, J. W. H., Schefuß, E., Herfort, L., Sinninghe Damsté, J. S. and  
760 Schouten, S.: A novel proxy for terrestrial organic matter in sediments based on branched  
761 and isoprenoid tetraether lipids, *Earth and Planetary Science Letters*, 224(1–2), 107–116,  
762 doi:10.1016/j.epsl.2004.05.012, 2004.

763 Horita, J. and Wesolowski, D. J.: Liquid-vapor fractionation of oxygen and hydrogen isotopes  
764 of water from the freezing to the critical temperature, *Geochimica et Cosmochimica Acta*,  
765 58(16), 3425–3437, doi:[http://dx.doi.org/10.1016/0016-7037\(94\)90096-5](http://dx.doi.org/10.1016/0016-7037(94)90096-5), 1994.

766 Hothorn, T., Bühlmann, P., Dudoit, S., Molinaro, A. and Van Der Laan, M. J.: Survival  
767 ensembles, *Biostatistics*, 7(3), 355–373, doi:10.1093/biostatistics/kxj011, 2006.

768 Hou, J., D'Andrea, W. J. and Huang, Y.: Can sedimentary leaf waxes record D/H ratios of  
769 continental precipitation? Field, model, and experimental assessments, *Geochimica et*  
770 *Cosmochimica Acta*, 72, 3503–3517, doi:10.1016/j.gca.2008.04.030, 2008.

771 Huguet, A., Fosse, C., Metzger, P., Fritsch, E. and Derenne, S.: Occurrence and distribution of  
772 extractable glycerol dialkyl glycerol tetraethers in podzols, *Organic Geochemistry*, 41(3),  
773 291–301, doi:10.1016/j.orggeochem.2009.10.007, 2010a.

774 Huguet, A., Fosse, C., Laggoun-Défarge, F., Toussaint, M. L. and Derenne, S.: Occurrence and  
775 distribution of glycerol dialkyl glycerol tetraethers in a French peat bog, *Organic*  
776 *Geochemistry*, 41(6), 559–572, doi:10.1016/j.orggeochem.2010.02.015, 2010b.

777 IAEA/WMO: Global Network of Isotopes in Precipitation. The GNIP Database., 2015.

778 IAEA/WMO: Global Network of Isotopes in Precipitation. The GNIP Database., 2018.

- 779 Jacob, H. and Sonntag, C.: An 8-year record of the seasonal- variation of  $^2\text{H}$  and  $^{18}\text{O}$  in  
780 atmospheric water vapor and precipitation at Heidelberg, *Tellus*, 43B(3), 291–300, 1991.
- 781 De Jonge, C., Hopmans, E. C., Zell, C. I., Kim, J. H., Schouten, S. and Sinninghe Damsté, J.  
782 S.: Occurrence and abundance of 6-methyl branched glycerol dialkyl glycerol tetraethers  
783 in soils: Implications for palaeoclimate reconstruction, *Geochimica et Cosmochimica*  
784 *Acta*, 141, 97–112, doi:10.1016/j.gca.2016.03.038, 2014.
- 785 Kahmen, A., Schefuß, E. and Sachse, D.: Leaf water deuterium enrichment shapes leaf wax *n*-  
786 alkane  $\delta\text{D}$  values of angiosperm plants I: Experimental evidence and mechanistic  
787 insights, *Geochimica et Cosmochimica Acta*, 111, 39–49, doi:10.1016/j.gca.2012.09.004,  
788 2013.
- 789 Knapp, D. R.: *Handbook of Analytical Derivatization Reactions*, John Wiley & Sons, New  
790 York, Chichester, Brisbane, Toronto, Singapore., 1979.
- 791 Konecky, B., Dee, S. G. and Noone, D. C.: WaxPSM: A Forward Model of Leaf Wax Hydrogen  
792 Isotope Ratios to Bridge Proxy and Model Estimates of Past Climate, *Journal of*  
793 *Geophysical Research: Biogeosciences*, 124, 2107–2125, doi:10.1029/2018JG004708,  
794 2019.
- 795 Laursen, E. V., Thomsen, R. S. and Cappelen, J.: Observed Air Temperature, Humidity,  
796 Pressure, Cloud Cover and Weather in Denmark - with Climatological Standard Normals,  
797 1961-90., 1999.
- 798 Levene, H.: Robust Tests for Equality of Variances, in *Contributions to Probability and*  
799 *Statistics: Essays in Honor of Harold Hotelling*, vol. 69, edited by I. Olkin, pp. 78–92,  
800 Stanford University Press, Palo Alto, California., 1960.
- 801 Liu, W. and Yang, H.: Multiple controls for the variability of hydrogen isotopic compositions  
802 in higher plant *n*-alkanes from modern ecosystems, *Global Change Biology*, 14(9), 2166–  
803 2177, doi:10.1111/j.1365-2486.2008.01608.x, 2008.
- 804 Liu, Y., Wang, J., Liu, D., Li, Z., Zhang, G., Tao, Y., Xie, J., Pan, J. and Chen, F.: Straw  
805 mulching reduces the harmful effects of extreme hydrological and temperature conditions  
806 in citrus orchards, *PLoS ONE*, 9(1), 1–9, doi:10.1371/journal.pone.0087094, 2014.
- 807 McInerney, F. A., Helliker, B. R. and Freeman, K. H.: Hydrogen isotope ratios of leaf wax *n*-  
808 alkanes in grasses are insensitive to transpiration, *Geochimica et Cosmochimica Acta*,  
809 75(2), 541–554, doi:10.1016/j.gca.2010.10.022, 2011.
- 810 Merlivat, L.: Molecular diffusivities of  $\text{H}_2^{16}\text{O}$ ,  $\text{HD}^{16}\text{O}$ , and  $\text{H}_2^{18}\text{O}$  in gases, *The Journal of*  
811 *Chemical Physics*, 69(6), 2864–2871, doi:http://dx.doi.org/10.1063/1.436884, 1978.
- 812 Mueller-Niggemann, C., Utami, S. R., Marxen, A., Mangelsdorf, K., Bauersachs, T. and  
813 Schwark, L.: Distribution of tetraether lipids in agricultural soils - Differentiation  
814 between paddy and upland management, *Biogeosciences*, 13(5), 1647–1666,  
815 doi:10.5194/bg-13-1647-2016, 2016.
- 816 Oppermann, B. I., Michaelis, W., Blumenberg, M., Frerichs, J., Schulz, H. M., Schippers, A.,  
817 Beaubien, S. E. and Krüger, M.: Soil microbial community changes as a result of long-  
818 term exposure to a natural  $\text{CO}_2$  vent, *Geochimica et Cosmochimica Acta*, 74(9), 2697–  
819 2716, doi:10.1016/j.gca.2010.02.006, 2010.
- 820 Pedentchouk, N. and Zhou, Y.: Factors Controlling Carbon and Hydrogen Isotope Fractionation  
821 During Biosynthesis of Lipids by Phototrophic Organisms, in *Hydrocarbons, Oils and*

- 822 Lipids: Diversity, Origin, Chemistry and Fate. Handbook of Hydrocarbon and Lipid  
823 Microbiology, edited by H. Wilkes, pp. 1–24, Springer, Cham., 2018.
- 824 Peterse, F., van der Meer, J., Schouten, S., Weijers, J. W. H., Fierer, N., Jackson, R. B., Kim,  
825 J. H. and Sinninghe Damsté, J. S.: Revised calibration of the MBT-CBT paleotemperature  
826 proxy based on branched tetraether membrane lipids in surface soils, *Geochimica et*  
827 *Cosmochimica Acta*, 96, 215–229, doi:10.1016/j.gca.2012.08.011, 2012.
- 828 Prietzel, J., Dechamps, N. and Spielvogel, S.: Analysis of non-cellulosic polysaccharides helps  
829 to reveal the history of thick organic surface layers on calcareous Alpine soils, *Plant and*  
830 *Soil*, 365(1–2), 93–114, doi:10.1007/s11104-012-1340-2, 2013.
- 831 R Core Team: R: A Language and Environment for Statistical Computing, [online] Available  
832 from: <https://www.r-project.org/>, 2015.
- 833 Rach, O., Brauer, A., Wilkes, H. and Sachse, D.: Delayed hydrological response to Greenland  
834 cooling at the onset of the Younger Dryas in western Europe, *Nature Geoscience*, 7(1),  
835 109–112, doi:10.1038/ngeo2053, 2014.
- 836 Rao, Z., Zhu, Z., Jia, G., Henderson, A. C. G., Xue, Q. and Wang, S.: Compound specific  $\delta D$   
837 values of long chain *n*-alkanes derived from terrestrial higher plants are indicative of the  
838  $\delta D$  of meteoric waters: Evidence from surface soils in eastern China, *Organic*  
839 *Geochemistry*, 40(8), 922–930, doi:<http://dx.doi.org/10.1016/j.orggeochem.2009.04.011>,  
840 2009.
- 841 Romero-Viana, L., Kienel, U. and Sachse, D.: Lipid biomarker signatures in a hypersaline lake  
842 on Isabel Island (Eastern Pacific) as a proxy for past rainfall anomaly (1942–2006AD),  
843 *Palaeogeography, Palaeoclimatology, Palaeoecology*, 350–352, 49–61,  
844 doi:10.1016/j.palaeo.2012.06.011, 2012.
- 845 Sachse, D., Radke, J. and Gleixner, G.: Hydrogen isotope ratios of recent lacustrine sedimentary  
846 *n*-alkanes record modern climate variability, *Geochimica et Cosmochimica Acta*, 68(23),  
847 4877–4889, doi:<http://dx.doi.org/10.1016/j.gca.2004.06.004>, 2004.
- 848 Sachse, D., Radke, J. and Gleixner, G.:  $\delta D$  values of individual *n*-alkanes from terrestrial plants  
849 along a climatic gradient – Implications for the sedimentary biomarker record, *Organic*  
850 *Geochemistry*, 37, 469–483, doi:10.1016/j.orggeochem.2005.12.003, 2006.
- 851 Sachse, D., Billault, I., Bowen, G. J., Chikaraishi, Y., Dawson, T. E., Feakins, S. J., Freeman,  
852 K. H., Magill, C. R., McInerney, F. A., van der Meer, M. T. J., Polissar, P., Robins, R. J.,  
853 Sachs, J. P., Schmidt, H.-L., Sessions, A. L., White, J. W. C. and West, J. B.: Molecular  
854 Paleohydrology: Interpreting the Hydrogen-Isotopic Composition of Lipid Biomarkers  
855 from Photosynthesizing Organisms, *Annual Reviews*, 40, 221–249,  
856 doi:10.1146/annurev-earth-042711-105535, 2012.
- 857 Schäfer, I. K., Lanny, V., Franke, J., Eglinton, T. I., Zech, M., Vysloužilová, B. and Zech, R.:  
858 Leaf waxes in litter and topsoils along a European transect, *SOIL*, 2, 551–564,  
859 doi:10.5194/soil-2-551-2016, 2016.
- 860 Schlotter, D.: The spatio-temporal distribution of  $\delta^{18}O$  and  $\delta^2H$  of precipitation in Germany -  
861 an evaluation of regionalization methods, Albert-Ludwigs-Universität Freiburg im  
862 Breisgau. [online] Available from: [http://www.hydrology.uni-](http://www.hydrology.uni-freiburg.de/abschluss/Schlotter_D_2007_DA.pdf)  
863 [freiburg.de/abschluss/Schlotter\\_D\\_2007\\_DA.pdf](http://www.hydrology.uni-freiburg.de/abschluss/Schlotter_D_2007_DA.pdf), 2007.
- 864 Schmidt, H.-L., Werner, R. A. and Roßmann, A.:  $^{18}O$  Pattern and biosynthesis of natural plant  
865 products, *Phytochemistry*, 58(1), 9–32, doi:<http://dx.doi.org/10.1016/S0031->



866 9422(01)00017-6, 2001.

867 Schmidt, H.-L., Werner, R. A. and Eisenreich, W.: Systematics of  $^2\text{H}$  patterns in natural  
868 compounds and its importance for the elucidation of biosynthetic pathways,  
869 *Phytochemistry Reviews*, 2(1–2), 61–85, doi:10.1023/B:PHYT.0000004185.92648.ae,  
870 2003.

871 Schouten, S., Hopmans, E. C. and Sinninghe Damsté, J. S.: The organic geochemistry of  
872 glycerol dialkyl glycerol tetraether lipids: A review, *Organic Geochemistry*, 54, 19–61,  
873 doi:10.1016/j.orggeochem.2012.09.006, 2013.

874 Schreuder, L. T., Beets, C. J., Prins, M. A., Hatté, C. and Peterse, F.: Late Pleistocene climate  
875 evolution in Southeastern Europe recorded by soil bacterial membrane lipids in Serbian  
876 loess, *Palaeogeography, Palaeoclimatology, Palaeoecology*, 449, 141–148,  
877 doi:10.1016/j.palaeo.2016.02.013, 2016.

878 Sessions, A. L., Burgoyne, T. W., Schimmelmann, A. and Hayes, J. M.: Fractionation of  
879 hydrogen isotopes in lipid biosynthesis, *Organic Geochemistry*, 30, 1193–1200, 1999.

880 Shapiro, S. S. and Wilk, M. B.: An Analysis of Variance Test for Normality, *Biometrika*,  
881 52(3/4), 591–611, doi:biomet/52.3-4.591, 1965.

882 Sternberg, L. S. L.: Comment on “Oxygen isotope ratios ( $^{18}\text{O}/^{16}\text{O}$ ) of hemicellulose-derived  
883 sugar biomarkers in plants, soils and sediments as paleoclimate proxy I: Insight from a  
884 climate chamber experiment” by Zech et al. (2014), *Geochimica et Cosmochimica Acta*,  
885 141, 677–679, doi:10.1016/j.gca.2014.04.051, 2014.

886 Strobl, C., Boulesteix, A. L., Zeileis, A. and Hothorn, T.: Bias in random forest variable  
887 importance measures: Illustrations, sources and a solution, *BMC Bioinformatics*, 8,  
888 doi:10.1186/1471-2105-8-25, 2007.

889 Strobl, C., Boulesteix, A. L., Kneib, T., Augustin, T. and Zeileis, A.: Conditional variable  
890 importance for random forests, *BMC Bioinformatics*, 9, 1–11, doi:10.1186/1471-2105-9-  
891 307, 2008.

892 Stumpp, C., Klaus, J. and Stichler, W.: Analysis of long-term stable isotopic composition in  
893 German precipitation, *Journal of Hydrology*, 517, 351–361,  
894 doi:10.1016/j.jhydrol.2014.05.034, 2014.

895 Sun, C. J., Zhang, C. L., Li, F. Y., Wang, H. Y. and Liu, W. G.: Distribution of branched  
896 glycerol dialkyl glycerol tetraethers in soils on the Northeastern Qinghai-Tibetan Plateau  
897 and possible production by nitrite-reducing bacteria, *Science China Earth Sciences*, 59(9),  
898 1834–1846, doi:10.1007/s11430-015-0230-2, 2016.

899 Swedish Meteorological and Hydrological Institute: SMHI Open Data Meteorological  
900 Observations., 2018.

901 Tipple, B. J., Berke, M. A., Hambach, B., Roden, J. S. and Ehleringer, J. R.: Predicting leaf  
902 wax *n*-alkane  $^2\text{H}/^1\text{H}$  ratios: Controlled water source and humidity experiments with  
903 hydroponically grown trees confirm predictions of Craig-Gordon model, *Plant, Cell and  
904 Environment*, 38(6), 1035–1047, doi:10.1111/pce.12457, 2015.

905 Tuthorn, M., Zech, M., Ruppenthal, M., Oelmann, Y., Kahmen, A., del Valle, H. F., Wilcke,  
906 W. and Glaser, B.: Oxygen isotope ratios ( $^{18}\text{O}/^{16}\text{O}$ ) of hemicellulose-derived sugar  
907 biomarkers in plants, soils and sediments as paleoclimate proxy II: Insight from a climate  
908 transect study, *Geochimica et Cosmochimica Acta*, 126, 624–634,

- 909 doi:<http://dx.doi.org/10.1016/j.gca.2013.11.002>, 2014.
- 910 Tuthorn, M., Zech, R., Ruppenthal, M., Oelmann, Y., Kahmen, A., del Valle, H. F., Eglinton,  
911 T., Rozanski, K. and Zech, M.: Coupling  $\delta^2\text{H}$  and  $\delta^{18}\text{O}$  biomarker results yields  
912 information on relative humidity and isotopic composition of precipitation - a climate  
913 transect validation study, *Biogeosciences*, 12, 3913–3924, doi:10.5194/bg-12-3913-  
914 2015, 2015.
- 915 Umweltbundesamt GmbH: Erhebung der Wassergüte in Österreich gemäß Hydrographiegesetz  
916 i.d.F. des BGBl. Nr. 252/90 (gültig bis Dezember 2006) bzw.  
917 Gewässerzustandsüberwachung in Österreich gemäß Wasserrechtsgesetz, BGBl. I Nr.  
918 123/06, i.d.g.F.; BMLFUW, Sektion IV / Abteilung 3 N. [online] Available from:  
919 <https://wasser.umweltbundesamt.at/h2odb/fivestep/abfrageQdPublic.xhtml> (Accessed 20  
920 September 2018), 2018.
- 921 Walker, C. D. and Brunel, J.-P.: Examining Evapotranspiration in a Semi-Arid Region using  
922 Stable Isotopes of Hydrogen and Oxygen, *Journal of Hydrology*, 118, 55–75, 1990.
- 923 Wang, C., Hren, M. T., Hoke, G. D., Liu-Zeng, J. and Garziona, C. N.: Soil *n*-alkane  $\delta\text{D}$  and  
924 glycerol dialkyl glycerol tetraether (GDGT) distributions along an altitudinal transect  
925 from southwest China: Evaluating organic molecular proxies for paleoclimate and  
926 paleoelevation, *Organic Geochemistry*, 107, 21–32,  
927 doi:10.1016/j.orggeochem.2017.01.006, 2017.
- 928 Wang, H., Liu, W., Zhang, C. L., Liu, Z. and He, Y.: Branched and isoprenoid tetraether (BIT)  
929 index traces water content along two marsh-soil transects surrounding Lake Qinghai:  
930 Implications for paleo-humidity variation, *Organic Geochemistry*, 59, 75–81,  
931 doi:10.1016/j.orggeochem.2013.03.011, 2013.
- 932 Weijers, J. W. H., Schouten, S., Spaargaren, O. C. and Sinninghe Damsté, J. S.: Occurrence  
933 and distribution of tetraether membrane lipids in soils: Implications for the use of the  
934  $\text{TEX}_{86}$  proxy and the BIT index, *Organic Geochemistry*, 37(12), 1680–1693,  
935 doi:10.1016/j.orggeochem.2006.07.018, 2006.
- 936 Weijers, J. W. H., Schouten, S., van den Donker, J. C., Hopmans, E. C. and Sinninghe Damsté,  
937 J. S.: Environmental controls on bacterial tetraether membrane lipid distribution in soils,  
938 *Geochimica et Cosmochimica Acta*, 71(3), 703–713, doi:10.1016/j.gca.2006.10.003,  
939 2007.
- 940 Weijers, J. W. H., Wiesenberg, G. L. B., Bol, R., Hopmans, E. C. and Pancost, R. D.: Carbon  
941 isotopic composition of branched tetraether membrane lipids in soils suggest a rapid  
942 turnover and a heterotrophic life style of their source organism(s), *Biogeosciences*, 7(9),  
943 2959–2973, doi:10.5194/bg-7-2959-2010, 2010.
- 944 Weijers, J. W. H., Steinmann, P., Hopmans, E. C., Schouten, S. and Sinninghe Damsté, J. S.:  
945 Bacterial tetraether membrane lipids in peat and coal: Testing the MBT-CBT temperature  
946 proxy for climate reconstruction, *Organic Geochemistry*, 42(5), 477–486,  
947 doi:10.1016/j.orggeochem.2011.03.013, 2011.
- 948 Xie, S., Pancost, R. D., Chen, L., Evershed, R. P., Yang, H., Zhang, K., Huang, J. and Xu, Y.:  
949 Microbial lipid records of highly alkaline deposits and enhanced aridity associated with  
950 significant uplift of the Tibetan Plateau in the Late Miocene, *Geology*, 40(4), 291–294,  
951 doi:10.1130/G32570.1, 2012.
- 952 Zech, M. and Glaser, B.: Compound-specific  $\delta^{18}\text{O}$  analyses of neutral sugars in soils using gas

953 chromatography-pyrolysis-isotope ratio mass spectrometry: problems, possible solutions  
954 and a first application, *Rapid Communications in Mass Spectrometry*, 23, 3522–3532,  
955 doi:10.1002/rem, 2009.

956 Zech, M., Rass, S., Buggle, B., Löscher, M. and Zöller, L.: Reconstruction of the late  
957 Quaternary paleoenvironments of the Nussloch loess paleosol sequence, Germany, using  
958 *n*-alkane biomarkers, *Quaternary Research*, 78(2), 226–235,  
959 doi:10.1016/j.yqres.2012.05.006, 2012a.

960 Zech, M., Kreutzer, S., Goslar, T., Meszner, S., Krause, T., Faust, D. and Fuchs, M.: Technical  
961 Note: *n*-Alkane lipid biomarkers in loess: post-sedimentary or syn-sedimentary?,  
962 *Discussions, Biogeosciences*, 9, 9875–9896, doi:10.5194/bgd-9-9875-2012, 2012b.

963 Zech, M., Tuthorn, M., Detsch, F., Rozanski, K., Zech, R., Zöller, L., Zech, W. and Glaser, B.:  
964 A 220 ka terrestrial  $\delta^{18}\text{O}$  and deuterium excess biomarker record from an eolian  
965 permafrost paleosol sequence, NE-Siberia, *Chemical Geology*,  
966 doi:10.1016/j.chemgeo.2013.10.023, 2013.

967 Zech, M., Mayr, C., Tuthorn, M., Leiber-Sauheitl, K. and Glaser, B.: Reply to the comment of  
968 Sternberg on “Zech et al. (2014) Oxygen isotope ratios ( $^{18}\text{O}/^{16}\text{O}$ ) of hemicellulose-  
969 derived sugar biomarkers in plants, soils and sediments as paleoclimate proxy I: Insight  
970 from a climate chamber experiment. *GCA, Geochimica et Cosmochimica Acta*, 141(0),  
971 680–682, doi:10.1016/j.gca.2014.04.051, 2014.

972 Zech, M., Zech, R., Rozanski, K., Gleixner, G. and Zech, W.: Do *n*-alkane biomarkers in  
973 soils/sediments reflect the  $\delta^2\text{H}$  isotopic composition of precipitation? A case study from  
974 Mt. Kilimanjaro and implications for paleoaltimetry and paleoclimate research, *Isotopes  
975 in Environmental and Health Studies*, 51(4), 508–524,  
976 doi:10.1080/10256016.2015.1058790, 2015.

977 Zech, R., Gao, L., Tarozo, R. and Huang, Y.: Branched glycerol dialkyl glycerol tetraethers in  
978 Pleistocene loess-paleosol sequences: Three case studies, *Organic Geochemistry*, 53, 38–  
979 44, doi:10.1016/j.orggeochem.2012.09.005, 2012c.

980